

Determining the helicity structure of third generation resonances

Andreas Papaefstathiou¹, Kazuki Sakurai²

¹*Institut für Theoretische Physik, Universität Zürich, Wintherturerstrasse 190,
CH-8057 Zürich, Switzerland*

²*Deutsches Elektronen Synchrotron DESY, Notkestrasse 85, D-22607 Hamburg,
Germany*

Email: andreas.papaefstathiou@physik.uzh.ch, kazuki.sakurai@desy.de

ABSTRACT: We examine methods that have been proposed for determining the helicity structure of decays of new resonances to third generation quarks and/or leptons. We present analytical and semi-analytical predictions and assess the applicability of the relevant variables in realistic reconstruction scenarios using Monte Carlo-generated events, including the effects of QCD radiation and multiple parton interactions, combinatoric ambiguities and fast detector simulation.

KEYWORDS: Hadronic Colliders, Beyond Standard Model.

Contents

1. Introduction	2
2. Variable definitions	3
2.1 Daughter-to-parent energy ratios, $x_{p,i}$	3
2.2 Semi-leptonic top variable, u	4
3. Applications	5
3.1 Flavour-changing Z'	6
3.2 $Z' \rightarrow \tau^+\tau^-$	14
3.3 Third-generation leptoquark pair-production	17
4. Conclusions	27
5. Acknowledgements	28
A. Angular variables	28
A.1 Definitions	28
A.2 Angular variables in the Z' flavour-changing model	28
B. The χ^2 between two histograms	30
C. Detector-level smearing	32
D. Alternative leptoquark decay: $S_{XY} \rightarrow t_R\bar{t}_L, t_L\bar{t}_R$	33
E. Matrix element for polarized top decay	33
F. Finite mass effects on top polarization	35
F.1 Production polarization	35
F.2 Polarization axis rotation effects	38
F.3 β distributions from Monte Carlo	39

1. Introduction

The third generation is thought to be intimately connected to the mechanism responsible for electroweak symmetry breaking due to the comparatively large top, tau and bottom Yukawa couplings. New, third generation resonances are further favoured in comparison to those of the first and second generation by flavour constraints, coming from experiments investigating flavour-changing processes [1].

Collider searches for new resonances decaying to third generation quarks or leptons (or both in the case of leptoquarks) are particularly challenging. This is primarily due to the fact that new physics signals have to compete against high QCD cross sections, which can immitate their topologies. But the properties of the third generation fermions, specifically their large masses and mixing angles, allow us to extract useful information from their decay products. The heaviest, the top quark, decays promptly before hadronization, and its decay products may consist of two or three jets (if the decay is hadronic) or to a jet plus a lepton and missing energy, requiring further reconstruction. Because of the promptness of the decay, its decay products possess angular distributions that are highly correlated to the top spin. The τ lepton can decay through several channels, again resulting in jets or leptons and missing energy, and various methods exist for identifying the resulting jets as having originated from a τ (i.e. τ -tagging). The b quark hadronizes before decay and produces B mesons which have relatively long lifetimes and thus produce displaced vertices. This allows for tagging those jets that originate from b quarks but washes away the effect of its helicity from the angular distributions of the associated daughter particles. Thus, the helicity of resonances containing a b quark has to be inferred by first determining the spin of the parent and sister particles.

Once new resonances are discovered, to fully determine the underlying theory and reconstruct the Lagrangian terms, both the spin and the structure of the couplings of the new resonances to standard model particles have to be determined. Determination of the helicity of top quarks has been investigated in detail in the past [2–4]. Several variables for determining the spin of top quarks have been proposed and QCD corrections to these variables have been calculated. Similar variables have also been proposed for τ leptons. Here we first review these and reproduce the relevant distributions, comparing them to results from a general-purpose Monte Carlo event generator, HERWIG++ [5].¹ In the case of hadronic top quark decays, the variables have thus far mostly been considered in the highly-boosted case. This allows for construction of the relevant distributions without requiring explicit event reconstruction. We relax this approximation and attempt to determine the usefulness of these variables in more realistic reconstruction situations. For simplicity, we first examine the applicability of these methods to a model containing a new heavy vector

¹In appendix A we also present a set of angular variables that complement the energy fraction variables given in the literature thus far.

boson, a Z' , which possesses decays to the third generation: either to a top and a light quark (specifically $t\bar{u}$, $\bar{t}u$) or a pair of τ leptons. We consider reconstruction of these topologies using mass-shell constraints which lead to a polynomial equation. In the latter case we also employ τ lepton vertex information. Subsequently we consider the more challenging case of a third-generation leptoquark model, focusing on pair production of these followed by decays to a top quark and a τ lepton. The reconstruction technique we employ is related to those presented in Ref. [6].

2. Variable definitions

2.1 Daughter-to-parent energy ratios, $x_{p,i}$

For the determination of the helicities of tops and taus, it is useful to define the energy fraction $x_{p,i} = \mathcal{E}_{p,i}/\mathcal{E}_p$, where \mathcal{E}_p is the energy of the parent particle and $\mathcal{E}_{p,i}$ is the energy of one of its daughter particles, i , both measured in the laboratory frame. These are formed for both the tau leptons and top quarks as:

$$\begin{aligned} x_{\tau,\text{jet}} &= \mathcal{E}_{\text{jet}}/\mathcal{E}_\tau, \\ x_{\text{top},b} &= \mathcal{E}_b/\mathcal{E}_{\text{top}}, \end{aligned} \quad (2.1)$$

respectively. For brevity, we will write x_{top} and x_τ to denote the preceding variables.

Analytic predictions for the energy ratios in the highly-boosted cases, where the boost factor, $\beta_k \equiv |\vec{p}_k|/E_k$, corresponding to particle k ($= t, \tau$), is taken to be unity, are shown in Fig. 1 for the τ lepton decay mode $\tau \rightarrow \pi\nu_\tau$ (left) and hadronic top (right). The distribution of x_{top} is cut-off at a maximum value of $x_{\text{top},\text{max}} = 1 - m_W^2/m_{\text{top}}^2 \sim 0.79$ and that of x_τ at a minimum value of $x_{\tau,\text{min}} = m_\pi^2/m_\tau^2$, as a result of the kinematic restrictions imposed by the mass of the W and the pion respectively. In the case of the τ , we show only the $\tau \rightarrow \pi\nu_\tau$ mode, for which $m_\pi \simeq 0.14$ GeV, which results in a small $x_{\tau,\text{min}}$.

The analytic forms of the distributions are given by [4]:²

$$\frac{1}{N} \frac{dN}{dx_\tau} = \frac{m_\tau^2}{m_\tau^2 - m_{\text{jet}}^2} \left(1 - \frac{1}{\beta_\tau} \frac{P_\tau(m_\tau^2 + m_{\text{jet}}^2)}{m_\tau^2 - m_{\text{jet}}^2} + \frac{1}{\beta_\tau} \frac{2P_\tau m_\tau^2}{m_\tau^2 - m_{\text{jet}}^2} x_\tau \right), \quad (2.2)$$

$$\frac{1}{N} \frac{dN}{dx_{\text{top}}} = \frac{m_{\text{top}}^2}{m_{\text{top}}^2 - m_W^2} \left(1 - \frac{1}{\beta_t} \kappa_b P_t + \kappa_b P_t \frac{1}{\beta_t} \frac{2m_{\text{top}}^2}{m_{\text{top}}^2 - m_W^2} x_{\text{top}} \right), \quad (2.3)$$

where $P_i = \pm 1$ (for $i = \tau, t$) represent right or left helicities of the τ or top and:

$$\kappa_b = -\frac{m_{\text{top}}^2 - 2m_W^2}{m_{\text{top}}^2 + 2m_W^2} \simeq -0.4, \quad (2.4)$$

²Note that in [4], Eq. (2.3) is missing a factor of $\frac{m_{\text{top}}^2}{m_{\text{top}}^2 - m_W^2}$ in the second term. The corresponding distributions, however, appear to have been constructed with the correct formulae.

is [4] the resolving power of the b -quark at leading order,³ m_{top} , m_W and m_τ are the top quark, W boson and τ lepton masses respectively. The limit $\beta_k \rightarrow 1$ allows us to investigate the distributions of reconstructed tops and taus without reference to the rest of the event, i.e. without explicit event reconstruction. The approximation is almost always good for τ leptons, and with the current beyond-the-standard model third generation limits rising as the LHC experiments produce more exclusion regions, it should ‘improve’ for most BSM models that include heavy particles that decay to tops. It is obvious from Eqs. (2.2) and (2.3) that the effect of $\beta_t \neq 1$ is to alter the predictions for the left- and right-handed distributions, modifying the straight-line form that appears in Fig. 1.

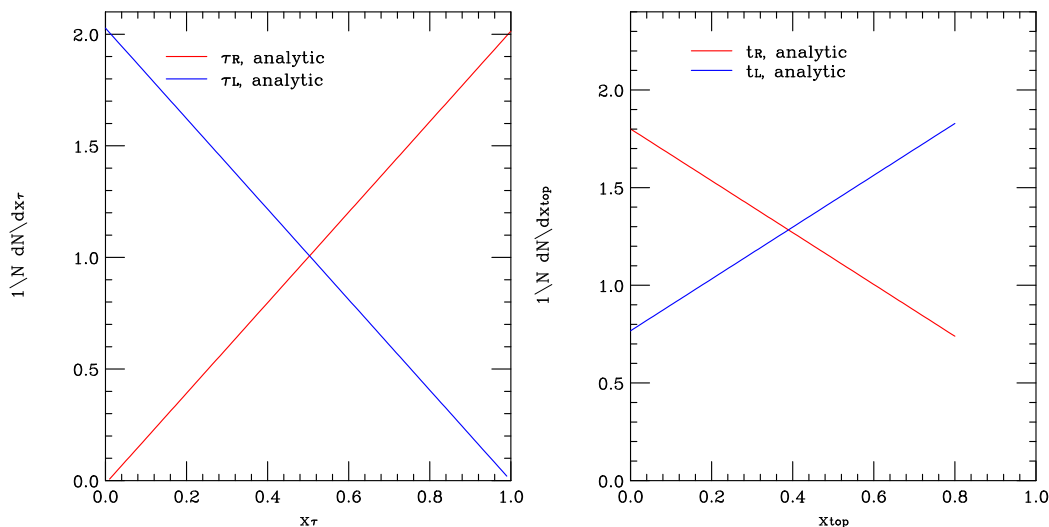


Figure 1: The predictions for the energy fractions $x_\tau = \mathcal{E}_{\text{jet}}/\mathcal{E}_\tau$ for the decay $\tau \rightarrow \pi\nu$ (left) and $x_{\text{top}} = \mathcal{E}_b/\mathcal{E}_{\text{top}}$ (right) in the highly-boosted cases.

The τ lepton can decay via multiple channels and each of these channels contributes to the total distribution. We do not attempt here to reproduce the analytic form of the distribution as this would require calculating the distributions of Eq. (2.2) corresponding to each decay mode and integrating over the distribution of the mass of the τ jet, m_{jet} , which would be varying when the τ decays to more than a single visible particle. Instead we present distributions constructed from the Monte Carlo-simulated decays of the τ lepton using the HERWIG++ event generator. We show the resulting distributions for the left- and right-handed highly-boosted taus in Fig. 2.

2.2 Semi-leptonic top variable, u

In the case of semi-leptonic top decays, $t \rightarrow b\ell\nu_\ell$, where a b -jet is tagged and an electron or muon is identified, we can calculate the fraction of the visible energy

³The authors of Ref. [7] present a study of polarisation observables at next-to-leading order with parton showers in H^-t and Wt production. They find that in those cases these observables are robust.

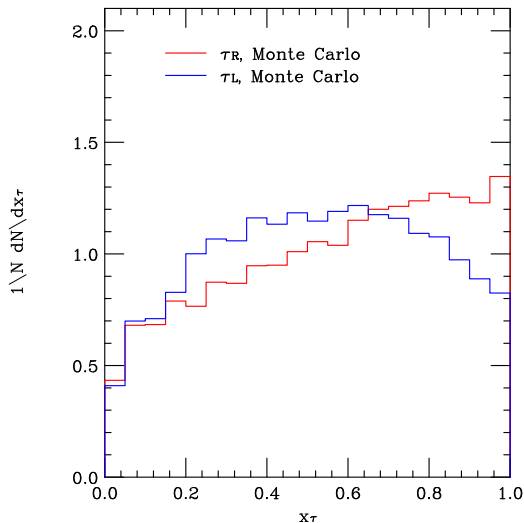


Figure 2: The Monte Carlo predictions for the energy fractions $x_\tau = \mathcal{E}_{\text{jet}}/\mathcal{E}_\tau$ for all the decay modes when the τ is highly boosted.

carried away by the lepton, u :

$$u = \frac{\mathcal{E}_\ell}{\mathcal{E}_\ell + \mathcal{E}_b} \quad (2.5)$$

The resulting distributions of the variable u for highly-boosted ($\beta_t \rightarrow 1$) [4] left- and right-handed tops are shown in Fig. 3. Highly-boosted Monte Carlo-generated curves are also shown for comparison, with and without final state radiation (FSR).⁴ The kink at $u = m_w^2/m_t^2 \sim 0.215$ is due to the fact that there exists a minimum possible value of the lepton energy in the top rest frame, given by $E_{\ell,\text{min}} = m_w^2/(2m_t)$, which arises when the lepton is anti-aligned with the top boost direction. The maximum value of the energy is $E_{\ell,\text{max}} = m_t/2$ and arises when the lepton is aligned with the boost direction. This is clarified in Fig. 4, where the schematic diagram demonstrates the decay of a top in its rest frame.

The variable u has the advantage that there is no need to explicitly reconstruct the top quarks in order to form it, even in the case of $\beta_t \neq 1$. As a result, it is expected to be less sensitive to the reconstruction systematics that may enter other energy fraction variables.

3. Applications

We examine a model of a heavy vector boson (Z') decaying to tops or taus and a scenario of pair-production of third generation scalar leptoquark states.

⁴Note that the curves of Fig. 2 in Ref. [4] seem to fit the FSR *on* case rather than the one obtained by integrating the differential width directly, which should fit the FSR *off* case.

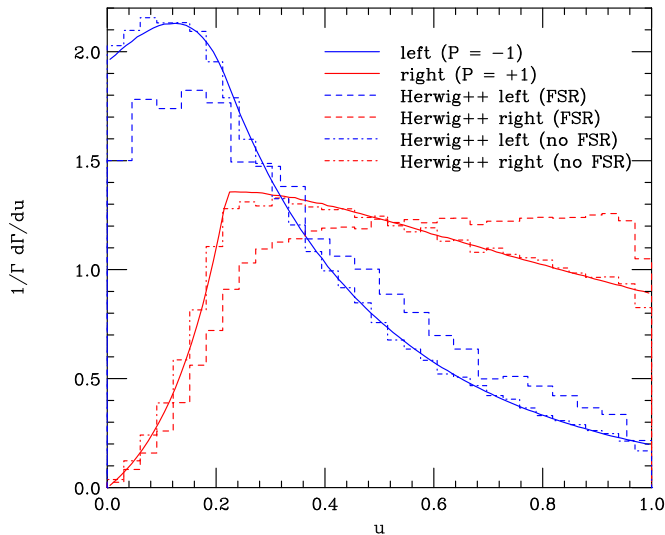


Figure 3: The distribution $1/\Gamma d\Gamma/du$ of the fraction of visible lab frame energy carried by the lepton in a highly-boosted semi-leptonic top, $u = \mathcal{E}_\ell/(\mathcal{E}_\ell + \mathcal{E}_b)$ is shown. The blue curve and red curves represent left- and right-handed top quarks respectively.

3.1 Flavour-changing Z'

We first examine the application of the variables x_{top} and u that have been defined in the previous sections, on a model of a Z' boson that possesses flavour-changing

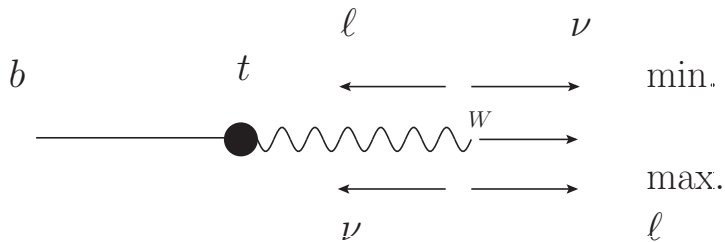


Figure 4: A schematic diagram of the decay of the top in its rest frame into a W and a b -quark, with subsequent decay of the W to a lepton and neutrino. The two configurations shown correspond to the minimum and maximum energy configurations of the lepton, corresponding to $E_{\ell,\text{min}} = m_w^2/(2m_t)$ and $E_{\ell,\text{max}} = m_t/2$ respectively. The minimum energy of the lepton causes the kink in the u variable distribution.

quark couplings, described by the Lagrangian density:

$$\begin{aligned} \mathcal{L} = & g_{Z'}^{tuR} Z'^{\mu} \bar{u}_R \gamma_{\mu} t_R + g_{Z'}^{tuL} Z'^{\mu} \bar{u}_L \gamma_{\mu} t_L \\ & + g_{Z'}^{uuR} Z'^{\mu} \bar{u}_R \gamma_{\mu} u_R + g_{Z'}^{uuL} Z'^{\mu} \bar{u}_L \gamma_{\mu} u_L + \text{h.c.} \quad , \end{aligned} \quad (3.1)$$

where $g_{Z'}^{tuL}$ and $g_{Z'}^{tuR}$ are the flavour-changing left- and right-handed parameters that we will be varying.

It is evident that the Z' bosons of this model would be produced at a hadron collider via light $u\bar{u}$ initial states. They will decay to both light $u\bar{u}$ and $t\bar{u}$ (and $u\bar{t}$). After discovery of such a state, for example in dijet resonance searches, determining the helicity structure of the $u\bar{u}Z$ vertex will be extremely challenging, if not impossible. Hence one would concentrate on determining the helicity structure of the vertex which involves the top quark.

3.1.1 Parton-level results

We consider a Z' described by the particular model given by the Lagrangian of Eq. (3.1), of mass 1.5 TeV, choosing either a purely left-handed third generation coupling: $g_{Z'}^{tuR} = 0$, $g_{Z'}^{tuL} = 1$ or a purely right-handed one: $g_{Z'}^{tuR} = 1$, $g_{Z'}^{tuL} = 0$, keeping in both cases $g_{Z'}^{uuR} = g_{Z'}^{uuL} = 1$.⁵ We show Monte Carlo results of the distributions of the variables x_{top} and u , for a 14 TeV LHC, in the dashed curves in Figs. 5 and 6. These results were obtained using parton-level events, ignoring initial- and final-state radiation, hadronization, and applying no rapidity or momentum cuts on the particles. Figures 5 and 6 also contain semi-analytic predictions that take into account the finite boost of the top quark in the lab frame (solid curves). The semi-analytic x_{top} distribution was produced by assuming that the cosine of the angle of the emitted b -quark in the top quark rest frame, $\cos \theta_b$, was distributed according to

$$P(\cos \theta_b) = (1 + P_t k_b \cos \theta_b) \quad , \quad (3.2)$$

with $\kappa_b \simeq -0.4$, and then boosted to the lab frame according to the top quark boost (β_t) distribution. The β_t distribution was extracted from the Monte Carlo event generator directly, but can be fitted using a Gaussian distribution, yielding identical results (see appendix F.3). Similarly, the u variable distribution was calculated first by distributing via a Monte Carlo technique the energy and z -momentum of the lepton in the top centre-of-mass frame (E_{ℓ} and p_{ℓ}^z respectively), according to the full matrix element (see appendix E) and then boosting to the lab frame using the top quark boost distribution. The variable u was then calculated by taking the ratio:

$$u = \frac{E_{\ell} + \beta_t p_{\ell}^z}{E_{\ell} + \beta_t p_{\ell}^z + E_b \beta_t p_b^z} \quad . \quad (3.3)$$

⁵This mass/coupling combination is currently being marginally excluded by results presented by the LHC experiments. Here we are only assessing the viability of the reconstruction variables and we are not concerned with the viability of the model itself.

In the case of the Z' the production and decay frames of the top quark are identical and hence there is no rotation angle between them (see appendix F). Furthermore, we ignore the mixing of helicities due to finite masses since the top quark is produced in association with a light quark which can be taken to be massless.⁶

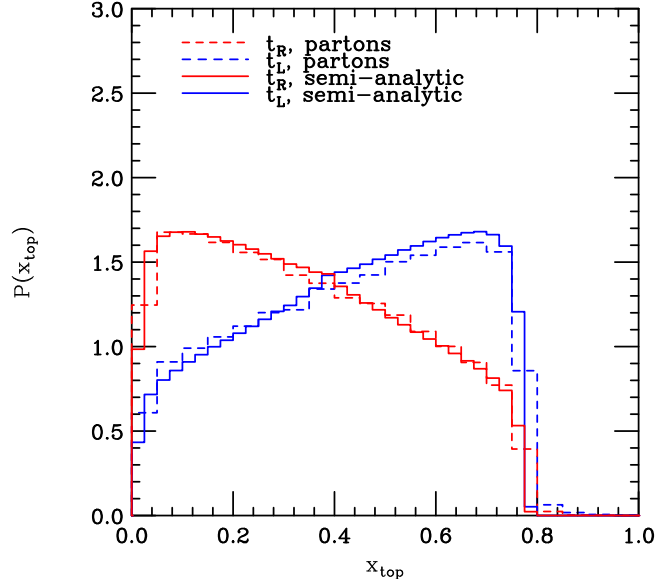


Figure 5: The x_{top} variable for left- or right-handed Z' bosons decaying to $u\bar{t}$ or $\bar{u}t$, at a 14 TeV LHC, obtained from parton-level events compared to a semi-analytic prediction as described in the main text.

3.1.2 Simulation and reconstruction

We will assume that the new resonances have been discovered, and that their mass has been measured to a satisfactory accuracy. We will also assume that the spin of the new resonance has been determined by measuring the angular distributions of the jets originating from the u and \bar{u} partons in the $u\bar{u}$ decay mode. It is necessary, however, to outline the details of the method for reconstructing events of a particular topology, for which we can form the variables we have been examining thus far at parton level.

We focus on LHC proton-proton collisions at 14 TeV, in which a Z' is exchanged, producing a u (or \bar{u})-quark and an anti-top (or top), with a subsequent semi-leptonic (restricted to e or μ) decay of the top. The topology is shown in Fig. 7. The $u\bar{t}$ and $\bar{u}t$ decay modes account for slightly less than $\sim 50\%$ of the total decay widths, if only one helicity (left- or right-handed) is present: $\Gamma_{Z',M=1.4 \text{ TeV}}(u\bar{t}/\bar{u}t) = 236 \text{ GeV}$. The leading order cross sections for the specific topology at a 14 TeV LHC are

⁶These effects are small in the case of the Z' model but have been calculated in the leptoquark case in the following section, where the reconstruction is explained in further detail.

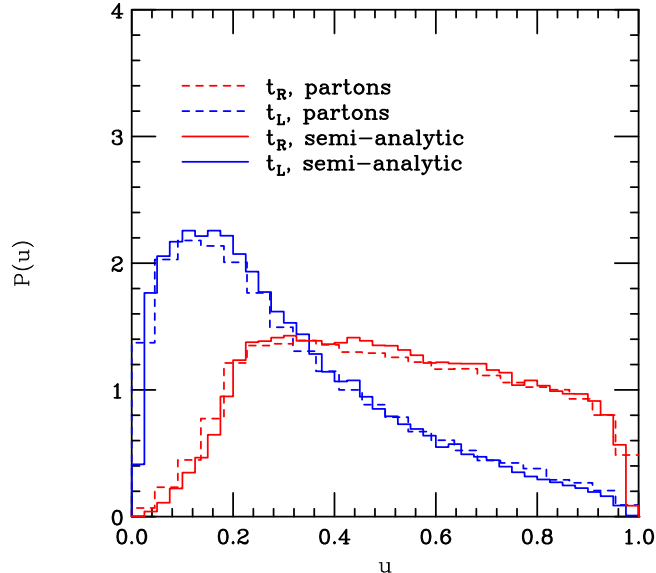


Figure 6: The u variable for left- or right-handed Z' bosons decaying to $u\bar{t}$ or $\bar{u}t$, at a 14 TeV LHC, obtained from parton-level events compared to a semi-analytic prediction as described in the main text.

$\sigma(Z' \rightarrow t\bar{u}/\bar{t}u \rightarrow b\ell^\pm\nu + \text{jet}) = 6.3$ pb, again, if only one helicity is present, and including the branching ratio of the top quark to electrons or muons.

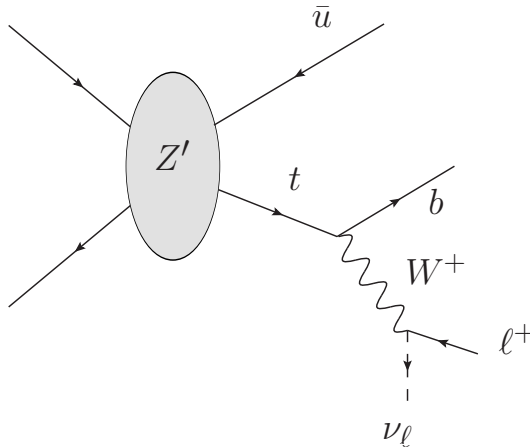


Figure 7: Production of $\bar{u}t$ from the exchange of a Z' and subsequent decay of the top into a leptonic W and a b -jet. This mode can be fully reconstructed if one applies the W mass shell condition, and chooses the solution which yields the ‘best’ top mass.

If a b -jet is tagged and a high- p_T lepton is found, along with the high- p_T jet originating from the u , the information left missing to fully reconstruct the final state are the three spatial momentum components of the neutrino (assuming massless neutrino). We can obtain the transverse components of the neutrino momentum to

a reasonable accuracy by assuming that they are equal to the components of the missing transverse momentum. Then, the only remaining missing information is the z -component of the neutrino momentum. In a hadron collider we do not possess any information on the initial z -momentum of the system. However if we assume that the neutrino and the lepton originated from the decay of an on-shell W boson, we may apply the following mass-shell condition on their four-momenta:

$$(p_\ell + p_\nu)^2 = m_W^2 \quad , \quad (3.4)$$

where p_ℓ and p_ν are the lepton and neutrino four-momenta respectively, and m_W is the on-shell W boson mass. This approximation is good, since the width of the W boson is small compared to its mass ($\Gamma_W \simeq 2.14$ GeV versus $M_W \simeq 80.40$ GeV), and leaves us with a quadratic equation for the z -component of the neutrino momentum. To pick one of the two solutions, we choose the one that also yields a top mass closest to the on-shell top mass, via:

$$m_{t,A/B}^2 = (p_\ell + p_{\nu,A/B} + p_b)^2 \quad , \quad (3.5)$$

where p_b is the b -jet four-momentum and $m_{t,A/B}$ is the top quark mass obtained by using the solutions for the neutrino momentum $p_{\nu,A/B}$. Once the ‘best’ solution is chosen, we possess all information required concerning the event, and we can thus calculate all the variables we have been examining at parton level.

The Z' model has been implemented and has been simulated using the HERWIG++ event generator with initial- and final-state radiation turned on, as well as hadronization. We simulated 10 fb^{-1} of data, a reasonable amount in a near- to mid-term LHC run at 14 TeV. The events were then processed through the Delphes detector simulation [8], where the following minimum cuts are applied to the reconstructed objects:

- $p_{T,\text{min}}$ for jets of 20.0 GeV.
- $p_{T,\text{min}}$ for electrons and muons of 10.0 GeV.

The default Delphes b -quark flat- p_T tagging efficiency was replaced by a more realistic function of jet transverse momentum, p_T , which has the form

$$P(p_{T,j}) = 0.08 + 0.006 \times p_{T,j} \times \exp(-3 \times 10^{-5} p_{T,j}^2) \quad . \quad (3.6)$$

See for example Ref. [9] for further details. The dependence on jet pseudorapidity remained flat. An additional cut requiring the total missing transverse energy to be greater than 20 GeV was applied. The rest represent the default settings present in the Delphes ATLAS detector card, where the trigerring simulation has been turned off. In this analysis, and the rest of this paper, we use the anti- k_T clustering algorithm with a radius parameter $R = 0.4$ to construct jets.⁷

⁷It is advantageous to use a smaller radius parameter for the anti- k_T clustering algorithm than the Delphes default one of $R = 0.7$, since underlying event and pile-up contaminations are expected to be approximately proportional to R^2 . See Ref. [10] for further details on jet algorithms and the underlying event.

The ‘best’ reconstructed top mass, after detector effects, was found to possess a peak at the correct on-shell top mass, ~ 174 GeV, with an approximately Gaussian distribution of width ~ 20 GeV. To illustrate the effect of the Delphes detector simulation, we show a comparison of results before and after Delphes processing in Figs. 8 and 9 for x_{top} and u respectively. The comparisons between the left- and right-handed variable distributions after detector effects are shown in Figs. 10 and 11. It is clear that, at least with the minimum cuts, the u variable performs well in discriminating between the pure left- or right-handed top quarks. The x_{top} variable is less different between the two top helicities, but the difference is still statistically significant. The advantage possessed by the variable u is clear: since no explicit reconstruction is required, the approximations that are associated with this process do not have a significant effect. As can be seen in the before/after plots in Figs. 8 and 9, the u variable is less sensitive to the experimental effects, which seem to ‘squeeze’ the distributions towards middle values of the energy fraction more dramatically in the case of x_{top} .

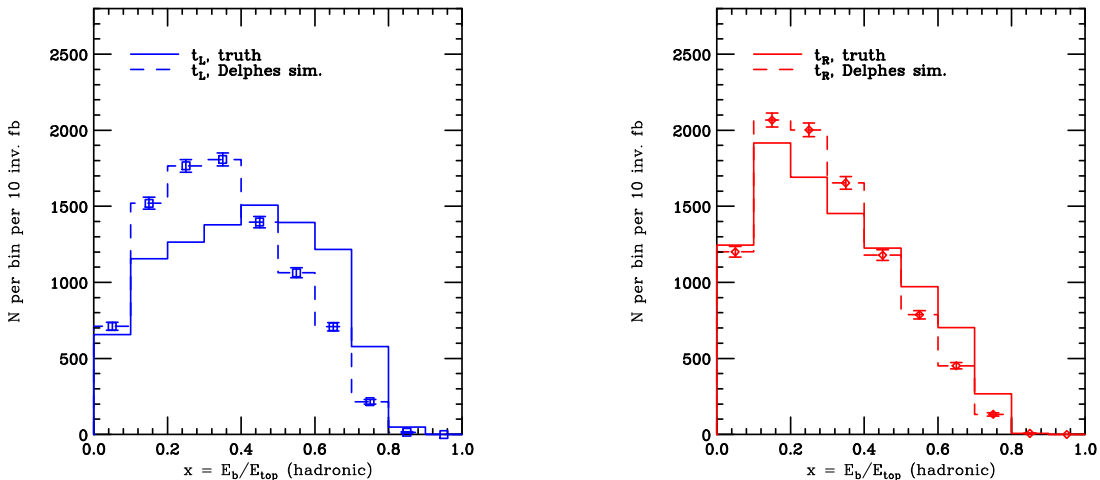


Figure 8: Shown in the figures is a comparison between the results obtained for the x_{top} variable for the 1.5 TeV flavour-changing Z' model *before* detector simulation (but applying all cuts and using equivalent jet-finding) and *after* the Delphes simulation for the left- and right- handed fermions (blue and red respectively).

To investigate the effect of higher transverse momentum cuts on the objects used in calculating these variables, we constructed two further sets of plots with higher cuts which we call ‘A’ and ‘B’ and are, respectively, $p_T > 30$ GeV and $p_T > 50$ GeV for both jets and leptons. The resulting distributions are shown in Figs. 12 and 13, where the set of cuts A is shown on the left, and set B on the right. Table 1 shows the value of $\chi^2/N_{\text{d.o.f.}}$ between the left- and right-handed distributions for the case of minimal cuts, as well as cuts ‘A’ and ‘B’.⁸ The value of $\chi^2/N_{\text{d.o.f.}}$ indicates how

⁸See appendix B for the definition of χ^2 in this case.

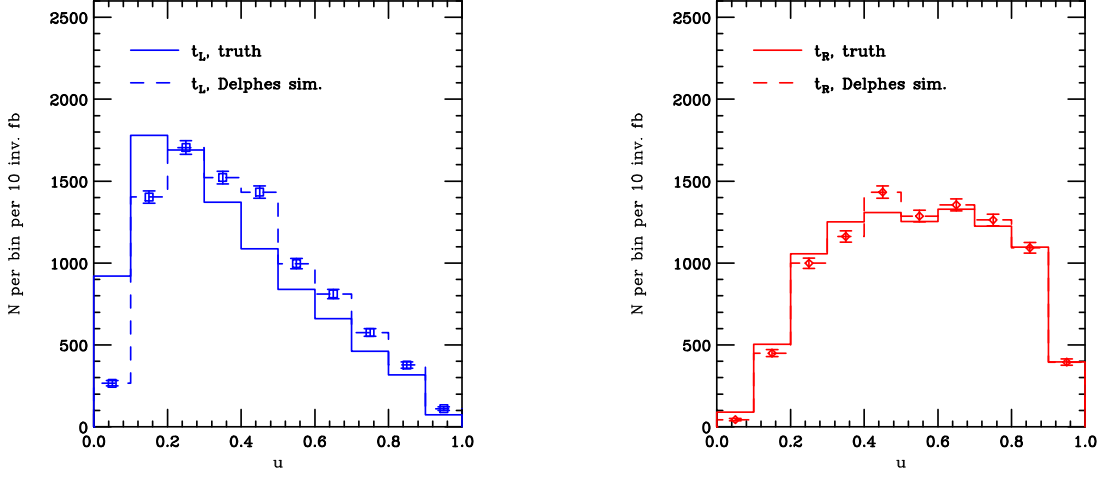


Figure 9: Shown in the figures is a comparison between the results obtained for the x_τ variable for the 1.5 TeV flavour-changing Z' model *before* detector simulation (but applying all cuts and using equivalent jet-finding) and *after* the Delphes simulation for the left- and right- handed fermions (blue and red respectively).

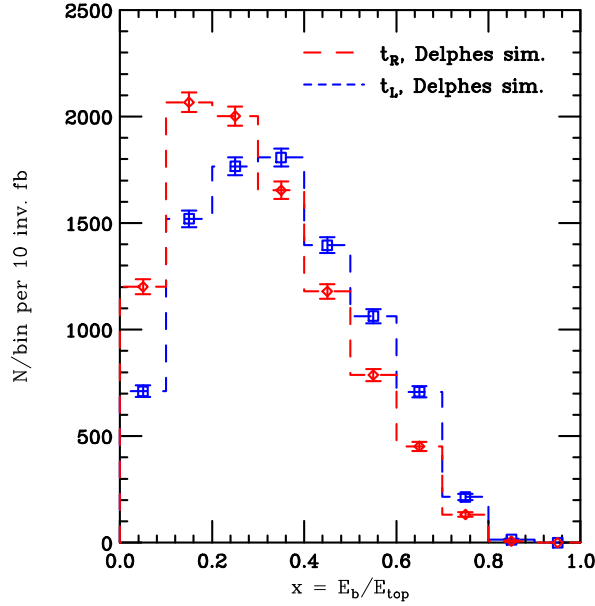


Figure 10: The x_{top} variable for a left- or right-handed Z' bosons decaying to $u\bar{t}$ or $\bar{u}t$, obtained from the reconstructed events for an LHC run at 14 TeV, with 10 fb^{-1} .

distinguishable the two distributions are statistically. It is evident that even in the case of higher cuts, discrimination in the specific scenario between the left- and right-handed modes is still possible. The higher cuts would also be beneficial for the

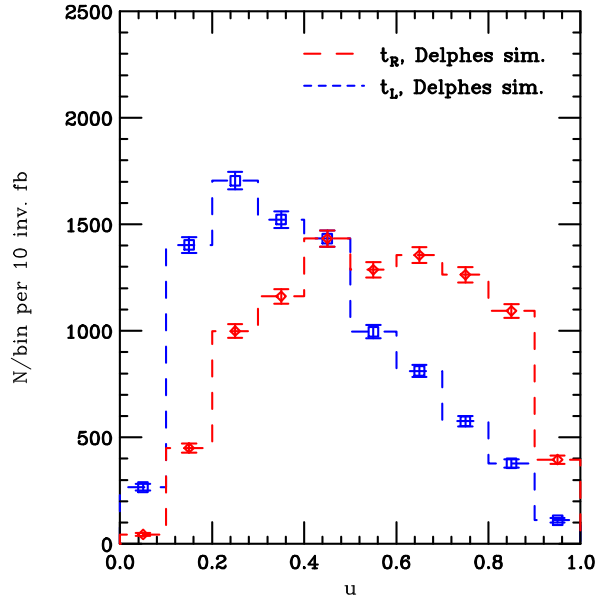


Figure 11: The u variable for a left- or right-handed Z' bosons decaying to $u\bar{t}$ or $\bar{u}t$, obtained from the reconstructed events for an LHC run at 14 TeV, with 10 fb^{-1} .

rejection of proton-proton pile-up,⁹ which would be detrimental at high instantaneous luminosity.

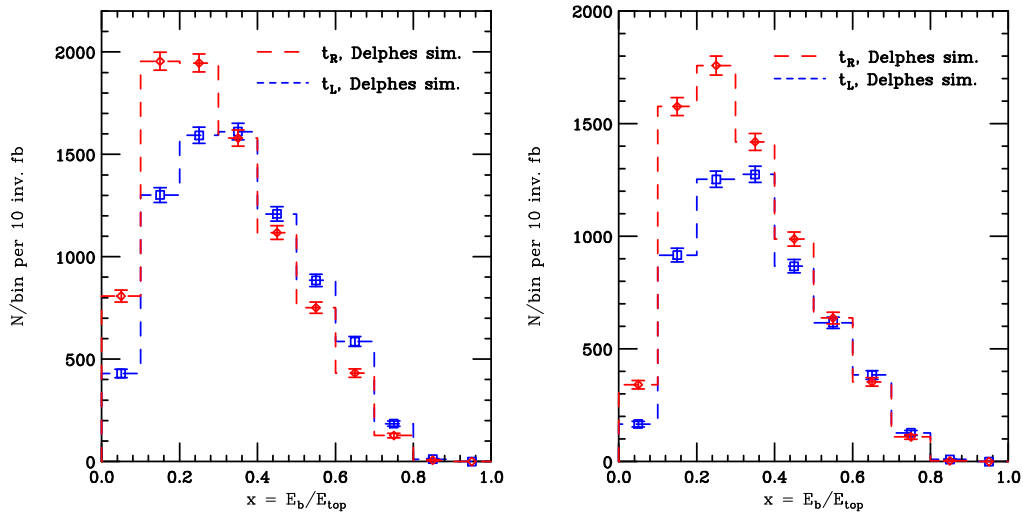


Figure 12: The x_{top} variable for a left- or right-handed Z' bosons decaying to $u\bar{t}$ or $\bar{u}t$, obtained from the reconstructed events for an LHC run at 14 TeV, with 10 fb^{-1} , with the set of cuts A (left) and B (right), as explained in the text.

⁹Pile-up is contamination originating from multiple secondary proton-proton collisions in the same bunch-crossing.

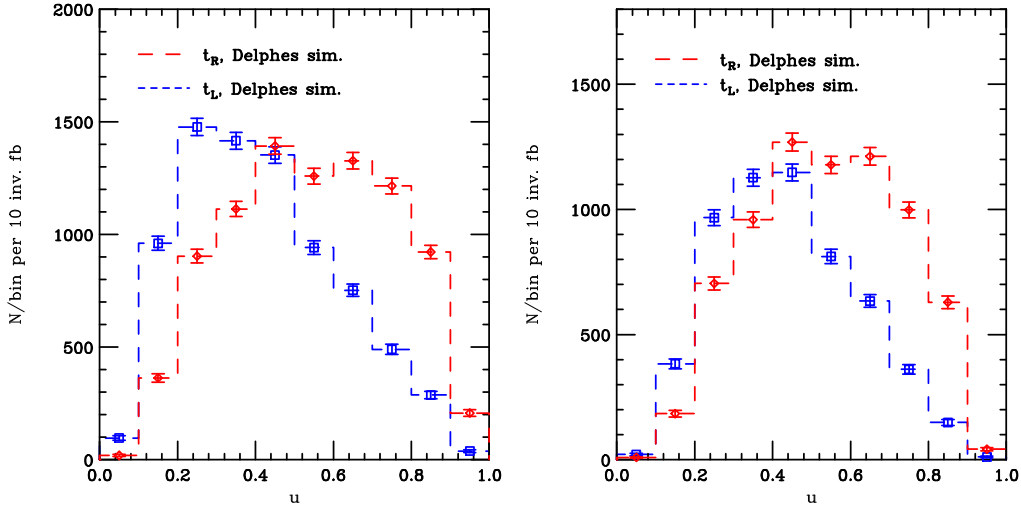


Figure 13: The u variable for a left- or right-handed Z' bosons decaying to $u\bar{t}$ or $\bar{u}t$, obtained from the reconstructed events for an LHC run at 14 TeV, with 10 fb^{-1} , with the set of cuts A (left) and B (right), as explained in the text.

Cut set	x_{top}	u
Min.	40.7	145.8
A	36.7	112.2
B	37.6	75.8

Table 1: The value of $\chi^2/N_{\text{d.o.f.}}$ between the left- and right-handed distributions in the Z' scenario for the three different sets of cuts. It is evident that the distributions are distinguishable even for the higher cuts, with the u variable distribution performing better in all cases.

3.2 $Z' \rightarrow \tau^+\tau^-$

Another interesting example, which we can use to examine the effectiveness of the energy ratio x_τ , is a model of a heavy Z' possessing a $\tau^+\tau^-$ decay mode. For this model, we define a Lagrangian density similar to the one given in the previous section:

$$\begin{aligned} \mathcal{L} = & g_{Z'}^{\tau\tau R} Z'^{\mu} \bar{\tau}_R \gamma_\mu \tau_R + g_{Z'}^{\tau\tau L} Z'^{\mu} \bar{\tau}_L \gamma_\mu \tau_L \\ & + g_{Z'}^{uuR} Z'^{\mu} \bar{u}_R \gamma_\mu u_R + g_{Z'}^{uuL} Z'^{\mu} \bar{u}_L \gamma_\mu u_L + \text{h.c.} , \end{aligned} \quad (3.7)$$

We examine discrimination between two cases, $Z' \rightarrow \tau_R^+ \tau_R^-$ ($g_{Z'}^{\tau\tau R} = 1$, $g_{Z'}^{\tau\tau L} = 0$) and $Z' \rightarrow \tau_L^+ \tau_L^-$ ($g_{Z'}^{\tau\tau R} = 0$, $g_{Z'}^{\tau\tau L} = 1$), using the x_τ variable defined in Eq. (2.1).

To compute the x_τ variable, one needs to reconstruct the neutrino energies from the τ decays. For this purpose, the authors in Ref. [11] have used the collinear approximation to reconstruct the neutrino momenta. In the collinear approximation, the neutrinos are assumed to be collimated to the associated τ -jets. This assumption is almost always good in cases of a heavy resonance decaying to τ leptons. Once the neutrino momentum directions are determined, the neutrino energies can be

calculated using the missing transverse momentum constraint:

$$\begin{pmatrix} p_{\text{miss}}^x \\ p_{\text{miss}}^y \end{pmatrix} = \begin{pmatrix} \sin \theta_{\text{jet1}} \cos \phi_{\text{jet1}} & \sin \theta_{\text{jet2}} \cos \phi_{\text{jet2}} \\ \sin \theta_{\text{jet1}} \sin \phi_{\text{jet1}} & \sin \theta_{\text{jet2}} \sin \phi_{\text{jet2}} \end{pmatrix} \begin{pmatrix} E_{\nu 1} \\ E_{\nu 2} \end{pmatrix}, \quad (3.8)$$

where θ_{jeti} , ϕ_{jeti} are the polar and azimuthal angles respectively, related to jet i , $p_{\text{miss}}^{x,y}$ are the missing transverse momentum components and $E_{\nu i}$ is the energy of neutrino i .

However, when the two jets are back-to-back, i.e. $\phi_{\text{jet1}} = \phi_{\text{jet2}} + \pi$, the inverse of the matrix in Eq.(3.8) becomes singular and any small mismeasurement on the missing transverse energy or jet momentum directions would cause a very large error on the reconstructed neutrino energy [12]. The back-to-back configuration is strongly preferable if a heavy resonance, such as the standard model Higgs boson or a Z' , is considered.

One can avoid the use of the collinearity assumption by instead using information on the τ decay vertices [13]. The most useful and best-measured attribute of these is their impact parameter. The impact parameter b is the displacement of a decay vertex in a direction perpendicular to that of the visible decay momentum, in this case the τ jet momentum \mathbf{p}_j . Then the invisible momentum \mathbf{p}_ν must lie in the $(\mathbf{b}, \mathbf{p}_j)$ plane, so we can write $\mathbf{p}_\nu = x\mathbf{b} + y\mathbf{p}_j$. For hadronic τ decays, the invisible momenta are carried by single neutrinos and so their four-momenta are fixed by x and y for each decay. In this section we focus on hadronic τ decays, by including a lepton veto in our event selection criteria. These four quantities are subject to two linear missing- p_T constraints and two quadratic τ mass-shell constraints, giving four (complex) solutions for the neutrino momenta.

These four complex solutions for the neutrino momenta allow us to compute the invariant mass of the τ pair. In Fig. 14, we plot the real part of the invariant mass, where we use the truth jet and missing transverse momenta for 10000 events. A distinct peak structure is seen at the input Z' mass of 1.5 TeV.

Unfortunately, our reconstruction method is still sensitive to the momentum mismeasurement. In Fig. 15, we show the hadronization and detector effects on the Z' mass reconstruction. In the left plot, the parton-level jets are replaced with the detector-level jets obtained from the Delphes simulation, in the middle plot only the parton-level missing transverse momentum is replaced with the detector-level one and in the right plot, we use all the detector-level objects. In all of the plots in Fig. 15, the true impact parameter was used. As can be seen, the peak structure is completely lost if one uses the detector objects. The event selection cuts here, and in all the results that follow in this section, are the default Delphes cuts for the ATLAS detector ($p_{T,\ell} > 10$ GeV, $p_{T,\text{jet}} > 20$ GeV) along with the addition of the lepton veto (in this case rejecting all events with an identified lepton).

However it is important to realise that, in the model we are considering, the Z' mass can be measured independently from the decay modes containing the light

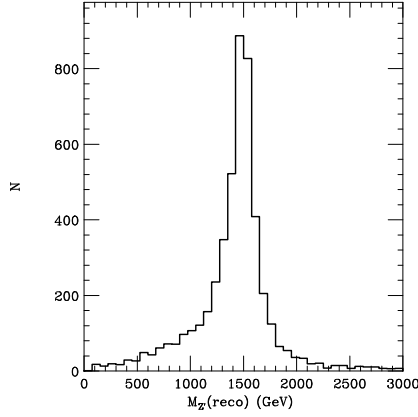


Figure 14: The real part of the complex solutions that arise after applying the two linear missing- p_T constraints and the two quadratic τ mass-shell constraints. A clear peak structure is seen at the input mass of 1.5 TeV.

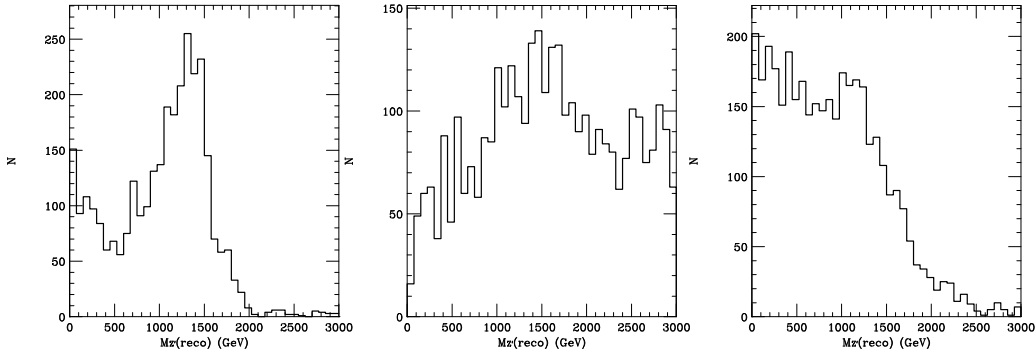


Figure 15: The distributions of the real part of the four complex solutions resulting from the reconstruction of the events after using detector-level jets instead of parton-level jets (left plot), detector-level missing transverse momentum instead of the true one (middle plot) and using completely detector-level objects (i.e. both for jets and MET, right plot). In all plots non-smearred τ vertices have been used.

quarks. In this case, we can use the mass shell constraint, $(p_{\tau_1} + p_{\tau_2})^2 = m_{Z'}^2$, as an extra condition to correct for the detector resolution. To accomplish this we construct the following likelihood function:

$$L_{\text{tot}} = L_{\text{detector}} \times L_{\text{phys}}, \quad (3.9)$$

where we have defined

$$\begin{aligned} L_{\text{detector}} &\equiv \prod_{i=1}^2 (P_{E_i} P_{\theta_i} P_{\phi_i}) \times P_E^{\text{miss}} \times P_{\phi}^{\text{miss}}, \\ L_{\text{phy}} &\equiv P_{m_{Z'}} \times \Theta(\text{Re}[E_{\nu_1}]) \times \Theta(\text{Re}[E_{\nu_2}]). \end{aligned} \quad (3.10)$$

The P_{E_i} , P_{θ_i} , P_E^{miss} , P_{ϕ}^{miss} are Gaussian probability functions centred at the origin, with arguments $(E_{j_i} - E_{j_i}^{\text{obs}})/E_{j_i}^{\text{obs}}$, $(\theta_{j_i} - \theta_{j_i}^{\text{obs}})$, $(p_{\text{Tmiss}} - p_{\text{Tmiss}}^{\text{obs}})/p_{\text{Tmiss}}^{\text{obs}}$, $(\phi_{p_{\text{Tmiss}}} - \phi_{p_{\text{Tmiss}}}^{\text{obs}})$, respectively. We also use the flat probability distribution, P_{ϕ_i} , for the $(\phi_i - \phi_i^{\text{obs}})$

with a range $[-0.9:0.9]$ so that the probability function matches the actual probability of mismeasurement, which is simulated by Delphes. The likelihood L_{phys} allows us to correct the mismeasured observable by requiring physical conditions with some probability. $P_{m_{Z'}}$ is a Gaussian probability function with an argument of $(m_{\tau\tau} - m_{Z'})$, where $m_{Z'}$ is the true Z' mass assumed to be measured through some other decay mode. $\Theta(x)$ is 1 if $x > 0$, 0 otherwise. The probability functions we use and the ones that appear in Delphes are shown in appendix C.

For each event, we generate 1000 pseudoevents, in which the observed momenta are slightly shifted in a random ‘direction’ according to the same probability function. We only keep the pseudo-event, i_{max} (corresponding to $L_{\text{tot}}^{\text{max}}$), that provides the maximum likelihood. We show the $\tau\tau$ invariant mass distribution obtained from i_{max} sample in Fig. 16.

In the left panel in Fig. 17, we show the relative difference between the true neutrino energy and the reconstructed neutrino energy by the likelihood method. As can be seen, the true neutrino energy is well reconstructed on an event-by-event basis with about 50% error. The right panel in Fig. 17 shows the reconstructed x_τ variable in this method, using 1 fb^{-1} of integrated luminosity at a 14 TeV LHC (corresponding to ~ 7000 events before cuts). The red (blue) solid histogram is obtained from $Z' \rightarrow \tau_R^+ \tau_R^-$ ($Z' \rightarrow \tau_L^+ \tau_L^-$) sample. The lepton veto in this realistic case was applied by requiring no leptons with $p_T > 10 \text{ GeV}$ in $|\eta| < 2.4$. The dashed histogram is the corresponding parton-level distribution of x_τ . It is obvious that the reconstructed x_τ has a very similar distribution to the parton-level one, and the difference between the left and right-handed x_τ distributions is visible even after the effects of detector resolution. The value of $\chi^2/N_{\text{d.o.f}}$ was found to be ~ 13.8 , indicating the high difference between the left- and right-handed x_τ histograms.

3.3 Third-generation leptoquark pair-production

Methods for reconstructing third-generation scalar leptoquark states in events where they were pair-produced have been studied in Ref. [6]. There, different mass variables were constructed and all the possible combinations of decay modes were studied, including QCD, detector and background effects. Here we will focus on the leptoquark types that can decay to a top quark and a tau lepton.

For a list of states that can decay to the $t\tau$ modes see Tables 1 and 2 in Ref. [6]. Instead of focusing on a specific leptoquark type, we consider a general scalar leptoquark which possesses a branching fraction of 1 to a top quark and a τ lepton. We call the leptoquarks of this type, with electromagnetic charge $\pm 5/3$, S_{LL} and S_{RR} , where the index indicates that the leptoquark will decay either to $t_L \tau_L$ or $t_R \tau_R$ respectively. In appendix D we consider leptoquarks of electromagnetic charge $\pm 1/3$ decaying to the mixed combinations $\bar{t}_R \tau_L$ or $\bar{t}_L \tau_R$ (S_{RL} and S_{LR} respectively). To obtain results for other scenarios of leptoquarks that decay into this mode, one has to simply rescale the results to account for the appropriate cross sections.

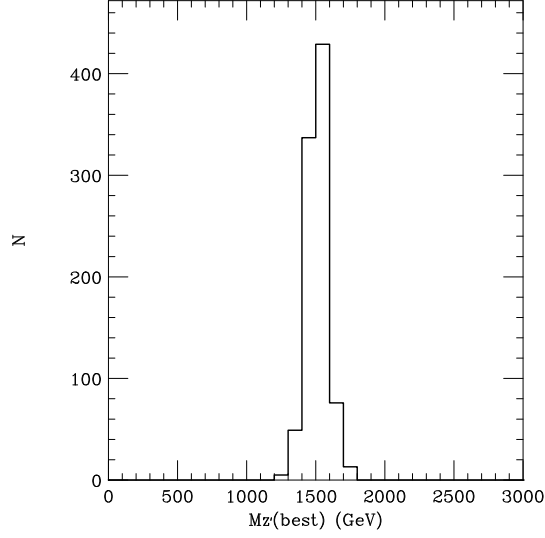


Figure 16: The $\tau\tau$ invariant mass of the maximum likelihood sample as described in the text. The distribution is sharply peaked at the input Z' mass of 1.5 TeV.

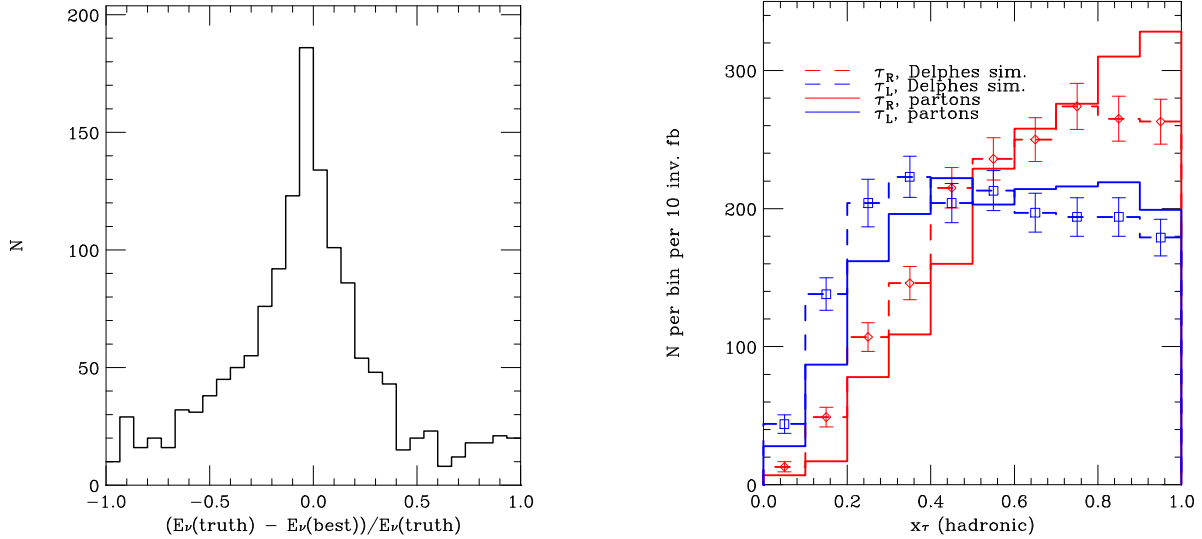


Figure 17: The relative difference between the true neutrino energy and the reconstructed neutrino energy using the likelihood method described in the text (left panel) and the resulting energy fraction, x_τ distributions for the purely left- and purely right-handed cases (right panel) for 1 fb^{-1} of integrated luminosity at 14 TeV.

3.3.1 Parton-level results

We produce Monte Carlo distributions of the variables outlined in section 2 for leptoquark states to compare to the predicted distributions at parton level. We do not present parton-level distributions for the τ , as the corresponding parton-level results have been already extracted from the Monte Carlo event generator itself and appear in Fig. 2.

The S_{XX} ($X \in \{R, L\}$) leptoquark can decay to $t\tau$ modes, described by the Lagrangian terms:

$$g_{RR}\bar{t}_R^c\tau_R S_{RR} + g_{LL}\bar{t}_L^c\tau_L S_{LL} + \text{h.c.} . \quad (3.11)$$

In the present study we set either $g_{RR} = 0, g_{LL} = 1$ (which we call purely left-handed) or vice versa: $g_{RR} = 1, g_{LL} = 0$ (which we call purely right-handed). The result for the highly-boosted x_{top} distributions obtained for purely left- and right-handed events in HERWIG++ is shown in Fig. 18 with the appropriate analytic prediction. The proton-proton centre-of-mass energy was set to 140 TeV and the leptoquark

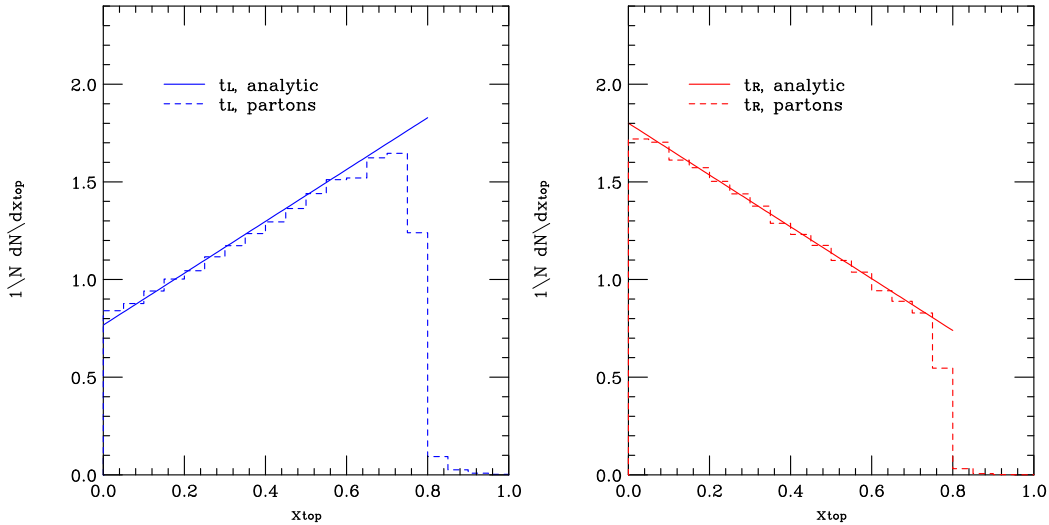


Figure 18: The Monte Carlo results for the energy fractions $x_{\text{top}} = \mathcal{E}_b/\mathcal{E}_{\text{top}}$ for $\tau_L t_L$ (left) and $\tau_R t_R$ (right) in the highly-boosted case. These are compared to analytical predictions as described in the text.

mass was set to 20 TeV, so that the top quarks are well within the highly-boosted region.

We also present the top quark results originating from the decay of scalar leptoquarks of mass 400 GeV at the LHC with pp COM energy of 14 TeV. Figures 19 and 20 show the left- and right-handed distributions of the variables x_{top} and u respectively, produced using the HERWIG++ Monte Carlo event generator and including semi-analytical predictions. These include the effects of the finite top and tau masses,

which introduce a mixture of helicities even though the Lagrangian terms are purely chiral, and the effect of the variation of the top boost in the lab frame, β_t .

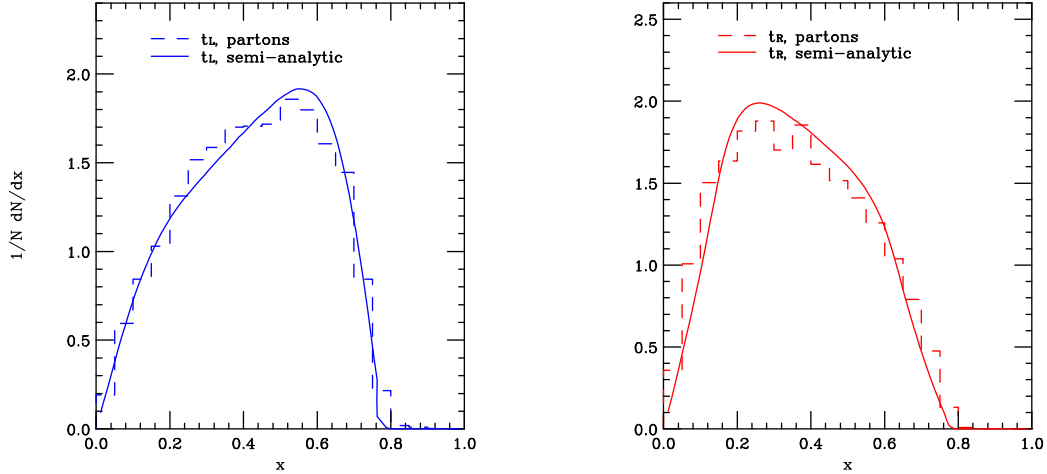


Figure 19: The results for the energy fractions $x_{\text{top}} = \mathcal{E}_b/\mathcal{E}_{\text{top}}$ for $\tau_L t_L$ (left) and $\tau_R t_R$ (right) for a 400 GeV mass at 14 TeV pp COM energy. These are compared to semi-analytical predictions as described in the text.

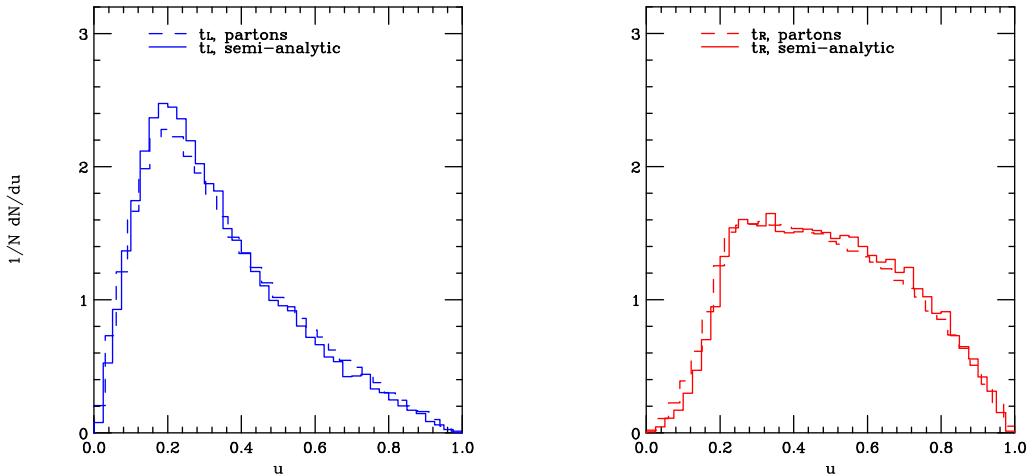


Figure 20: The Monte Carlo results for the energy fractions $u = \frac{\mathcal{E}_\ell}{\mathcal{E}_\ell + \mathcal{E}_b}$ for $\tau_L t_L$ (left) and $\tau_R t_R$ (right) for a 400 GeV mass at 14 TeV pp COM energy. These are compared to semi-analytical predictions as described in the text.

The semi-analytical predictions have been produced using Monte Carlo techniques as described in section 3.1: the x_{top} distribution was produced by distributing $\cos \theta_b$ according to $P(\cos \theta_b) = (1 + P_t k_b \cos \theta_b)$, and the β_t distribution for the top quark boost was extracted from the Monte Carlo event generator (see appendix F.3). Using either a fit or the extracted distribution yields indistinguishable results.

Since the boost of the parent leptoquark in the lab frame and the daughter top quark in the lab frame are correlated, we extracted the two-dimensional distribution $P(\beta_p, \beta_t)$ from the HERWIG++ event generator (appendix F.3). In principle, the β_p distribution can be calculated for any process using the hadron parton density functions and an assumption for the hard process, in this case scalar $SU(3)_c$ triplet pair-production. The variable β_p in the case of pair-produced leptoquarks of mass M_{LQ} is then related to the centre-of-mass energy by $\beta_p = \sqrt{1 - 4M_{LQ}^2/Q^2}$. The method described in appendix F was then used to calculate the detected polarization of the top for each event. The effect reduces the polarization on average by less than 10%. The mixing of helicities due to the mass of the top quark is low (less than 0.1%) due to the fact that it is produced along with a very light fermion (the τ) in the case we are considering.

The u distribution was produced in a similar way, using the full polarized top matrix element (see appendix E). The W decay to a lepton and a neutrino was set up in the W rest frame using a polar angle $\bar{\theta}$ and an azimuthal angle $\bar{\phi}$ for the lepton and neutrino momenta. These were then boosted to the top frame, where the b quark and W boson momenta were distributed in the top frame using a single polar angle $\tilde{\theta}$.¹⁰ The W mass was distributed according to a Breit-Wigner, centred about m_W . The effect of the W width was found to be small. The distribution was then calculated by taking the ratio:

$$u = \frac{E_\ell + \beta_t p_\ell^z}{E_\ell + \beta_t p_\ell^z + E_b \beta_t p_b^z}, \quad (3.12)$$

where E_ℓ and E_b are the lepton and b -quark energies in the top rest frame and β_t is again the boost of the top, sampled from either from the fit (Eq. (F.17)) or the Monte Carlo distribution directly. The calculations of the effect of the finite top and τ masses in the decay of a scalar and the relation of the top axis of polarization and direction of motion follow those which appear in Ref. [4] and are described briefly in appendix F.

3.3.2 Simulation and reconstruction

A mass reconstruction strategy for the $(t\tau)(t\tau)$ decay mode is described in Ref. [6]. The reconstruction there focuses on the modes $\bar{S}(S) \rightarrow bj j_1 \nu_1$, $S(\bar{S}) \rightarrow b\ell \nu_3 j_2 \nu_2$. We call this the hadronic/semi-leptonic mode, as opposed to the fully hadronic mode which we will examine below. An important assumption, that we have already discussed in section 3.2, which allowed for the full reconstruction of this decay mode, is the collinearity of the decay products of the tau leptons, owing to the fact that they

¹⁰Initially there are 9 degrees of freedom coming from the momenta of the b , ℓ and ν . Four-momentum conservation offers four constraints and the mass-shell conditions for the top and W offer a further two.

are highly-boosted in the lab frame. This has been tested for different leptoquark masses in Ref. [6]. The assumption can be applied by the relation $p_{\tau_i} = z_i p_{j_i}$, where $i = 1, 2$ and the energy ratios imply that $z_i \geq 1$.¹¹ In Ref. [6] a quartic equation was obtained for the energy ratio z_2 and each solution is a unique reconstruction of the whole event. This method provides a clean way to discriminate the leptoquark signal from the background. However, both the number of events, and the quality of the individual four-momenta reconstruction is insufficient for a detailed study of the helicities of the top and τ . Here we focus instead on the topology that contains two fully hadronic tops, shown in Fig. 21.

The signal was generated using the HERWIG++ event generator, including initial- and final-state radiation (ISR and FSR), hadronization effects and the underlying event (multiple parton interactions) and the detector response was simulated using the Delphes package with the default ATLAS settings, modified by the b -tagging function of Eq. (3.6), without the trigger simulation. Here, we also used the anti- k_T algorithm with radius parameter $R = 0.4$. The following cuts were applied on data corresponding to an integrated luminosity of 100 fb^{-1} at 14 TeV:

- A minimum of 6 jets (since the jets originating from the W could be identified as one jets).
- The missing transverse momentum in the event, $E_T^{\text{miss}} > 20 \text{ GeV}$.
- Two τ -tagged jets *and* two b -tagged jets, all with the extra requirement that they have $p_{T,\tau} > 20 \text{ GeV}$.

Note that these are the minimal cuts that one could impose in principle experimentally, and are lower than those imposed in the reconstruction techniques proposed in Ref. [6].

Full reconstruction of the decay topology shown in Fig. 21 is possible, since we would only be missing the neutrino momenta originating from the decays of the highly-boosted τ leptons, once the hadronic tops have been reconstructed. Using the approximation for the tau collinearity, one is left with only two unknowns, the z_1 and z_2 energy fractions. By assuming that the x and y components of the missing momentum are equal to those of the sum of the two neutrino components, we obtain two linear equations:

$$\begin{aligned} p_{\text{miss}}^x &= p_{j_1}^x(z_1 - 1) + p_{j_2}^x(z_2 - 1) , \\ p_{\text{miss}}^y &= p_{j_1}^y(z_1 - 1) + p_{j_2}^y(z_2 - 1) , \end{aligned} \tag{3.13}$$

¹¹Note that, in the events we are considering the leptoquarks are always boosted in the laboratory frame, so there is no issue with back-to-back τ leptons as the one which previously appeared in section 3.2.

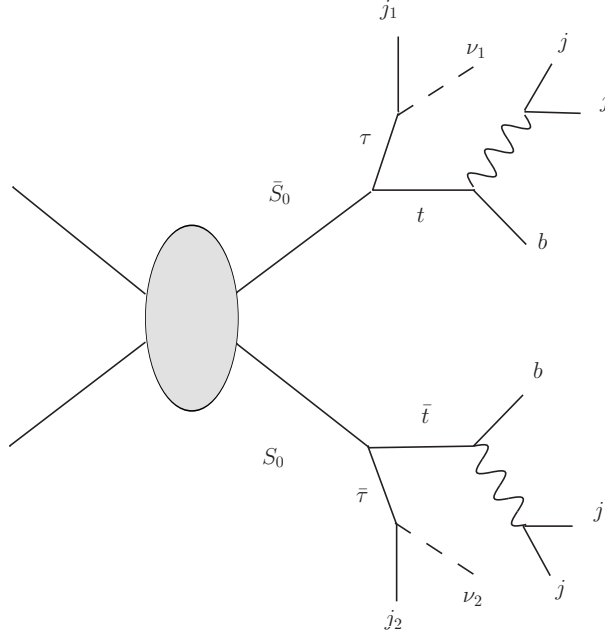


Figure 21: Pair-production of a leptoquark pair with decay to $(t\tau)(t\tau)$, followed by two fully hadronic top decays.

which can be solved to give:

$$\begin{aligned}
 z_1 &= 1 + \frac{p_{j2}^y p_{\text{miss}}^x - p_{j2}^x p_{\text{miss}}^y}{p_{j1}^x p_{j2}^y - p_{j2}^y p_{j1}^x}, \\
 z_2 &= 1 - \frac{p_{j1}^y p_{\text{miss}}^x - p_{j1}^x p_{\text{miss}}^y}{p_{j1}^x p_{j2}^y - p_{j2}^y p_{j1}^x}.
 \end{aligned}
 \tag{3.14}$$

The invariant mass of each of the two leptoquarks may be written as $m_S^2 = (p_t + p_\tau)^2$, resulting in the following expression:

$$m_S^2 = 2z_i p_{ti} \cdot p_{ji} + m_{\text{top}}^2,
 \tag{3.15}$$

where we have neglected the τ mass term. Using Eqs. (3.14), we obtain two values of m_S per event. Since this analysis would be performed *after* potential discovery, we would already have a measurement of the mass of the leptoquark. This would allow for elimination of backgrounds that may contribute and alter the energy fraction distributions.

To assess the possibility of measuring the helicity of the top quarks and tau leptons, we generated 100 fb^{-1} of a fully hadronic sample for purely left-handed or right-handed couplings and passed them through the Delphes simulation. We then analysed events which contained 2 τ -tagged jets and 2 b -tagged jets. We looked for 1 or 2 jets which reconstructed the top mass in conjunction with the tops, within an

80 GeV window.¹² For completeness, we show in Fig. 22 the resulting reconstructed masses using the above method, without any attempt to optimise the resulting values. Each event was given weight 1, since there are 4 entries per event due to the combinatoric ambiguities arising from the pairing of the top quarks and the τ leptons. To obtain the best value of the variables x_{top} and x_τ , we choose the combination

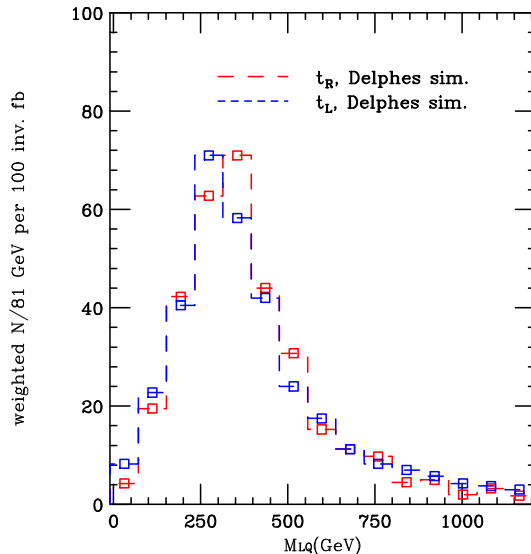


Figure 22: Mass reconstruction in the fully hadronic mode for the purely left- and right-handed cases for an integrated luminosity of 100 fb^{-1} . There are 4 entries per event, weighted by 0.25 each.

which yields the best leptoquark mass, that is, the one closest to the true mass. We then obtain two values of the x_τ variable: $x_{\tau,1/2} = 1/z_{1/2}$ and two values of the x_{top} variable by using the energies of the two b -jets and the reconstructed top energy. A comparison between the results obtained *before* detector simulation, but applying all cuts and using equivalent jet-finding, and after the Delphes simulation, is shown in Figs. 23 and 24 on the left- and right-handed fermions, for the variables x_{top} and x_τ . The results without detector simulation have been normalised to the number of events resulting after Delphes simulation. The differences that arise at low and high energy fractions and can be attributed primarily to the efficiency of the tagging algorithms and the overall differences to the smearing of the four-momenta due to the simulation of the response of the detector. Comparisons of the Delphes results are shown in Figs. 25 and 26 respectively for the purely left- and right-handed cases.

¹²To further improve the ‘top-tagging’ capabilities of the analysis, one can employ a more advanced tagging algorithm such as the one presented in Ref. [14]. For our purposes, the simpler reconstruction method of requiring combinations of jets to satisfy the top mass is sufficient to provide good results.

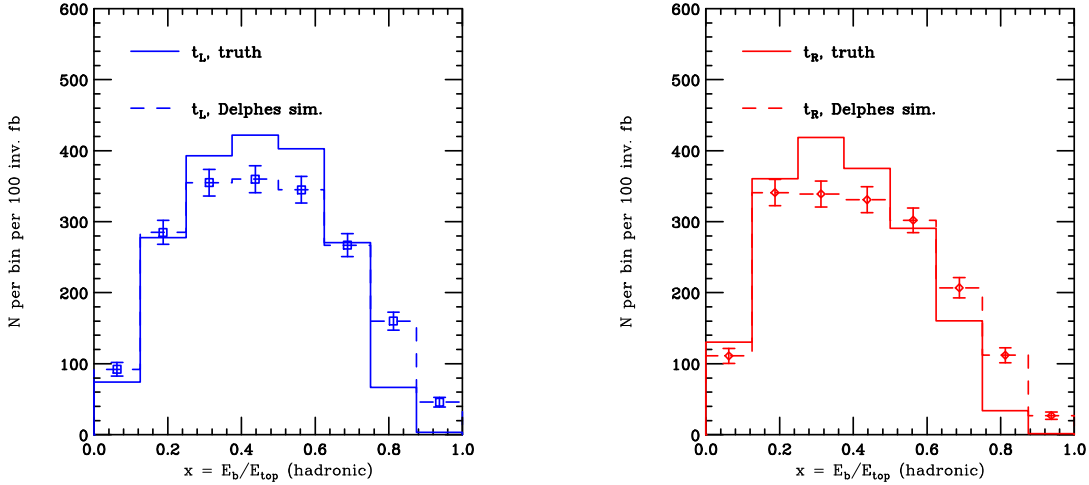


Figure 23: Shown in the figures is a comparison between the results obtained for the x_{top} variable for 400 GeV leptiquarks *before* detector simulation (but applying all cuts and using equivalent jet-finding) and after the Delphes simulation for the left- and right-handed fermions (blue and red respectively).

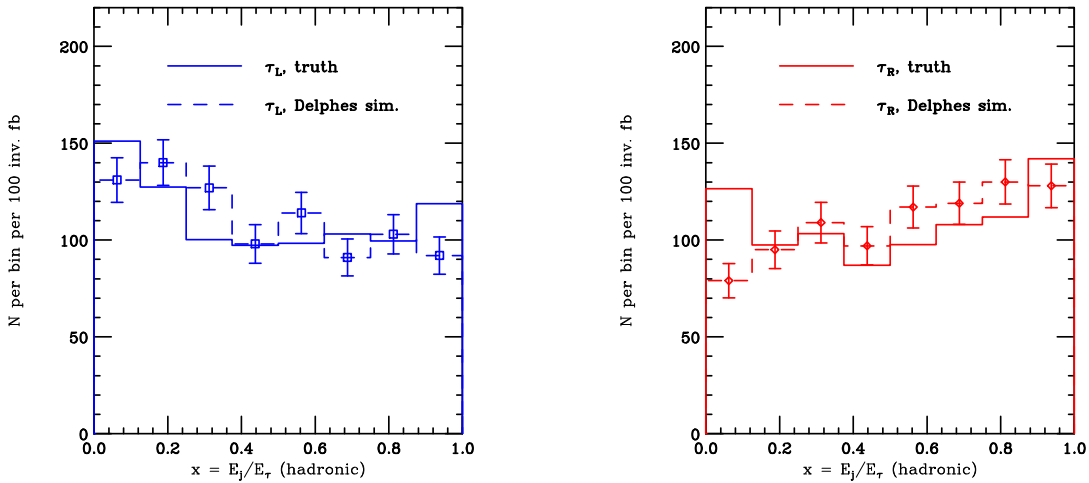


Figure 24: Shown in the figures is a comparison between the results obtained for the x_τ variable for 400 GeV leptiquarks *before* detector simulation (but applying all cuts and using equivalent jet-finding) and after the Delphes simulation for the left- and right-handed fermions (blue and red respectively).

To assess the discrimination capabilities of the distributions, we calculated the $\chi^2/N_{\text{d.o.f.}}$ between the left- and right-handed distributions. To investigate the effect of higher transverse momentum cuts, we re-ran the analysis with two higher p_T cuts on the jets and the missing transverse momentum: set ‘A-prime’ with p_T and $\cancel{E}_T > 25$ GeV and set ‘A’ with p_T and $\cancel{E}_T > 30$ GeV. The results are shown in

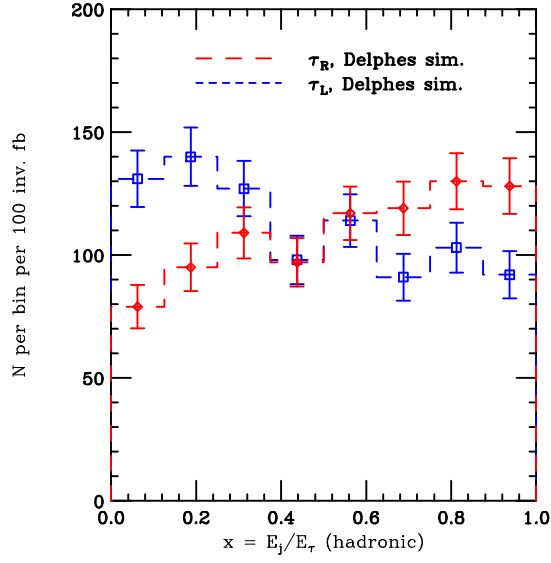


Figure 25: The x_τ variable for left- or right-handed $t\tau$ for an integrated luminosity of 100 fb^{-1} modes originating from the reconstructed events in the fully hadronic case, using the method described in the text.

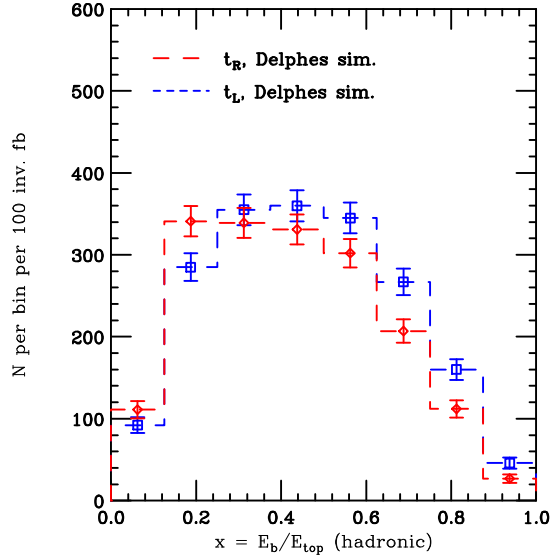


Figure 26: The x_{top} variable for left- or right-handed $t\tau$ for an integrated luminosity of 100 fb^{-1} modes originating from the reconstructed events in the fully hadronic case, using the method described in the text.

Table 2.

Cut set	x_{top}	x_{τ}
Min.	4.0	4.5
A-prime	2.9	3.8
A	1.9	2.8

Table 2: The value of $\chi^2/N_{\text{d.o.f.}}$ between the left- and right-handed distributions in the leptoquark $t\tau$ decay scenario, for the three different sets of cuts. It is evident that the distributions become more difficult to distinguish for the higher cuts at the given integrated luminosity of 100 fb^{-1} .

4. Conclusions

We have investigated variables that have been defined for the purpose of determining the helicity of top quarks and tau leptons in a more realistic setting than what has been done so far in the literature. We first examined these analytically in the highly-boosted case, where no explicit reconstruction of the event would be necessary to observe the given distributions. Subsequently we focused on two specific models: one containing a new heavy vector boson, Z' , with decays to either a light jet and a top quark or two taus, and a specific scenario in scalar leptoquark pair-production, in which the decay of both leptoquarks is into a top quark and a τ lepton. We examined the flavour-changing Z' model at parton level, producing the relevant distributions semi-analytically and comparing these directly to the Monte Carlo-generated distributions. We considered experimental and reconstruction effects for the case of a LHC at proton-proton centre-of-mass energy of 14 TeV and 10 fb^{-1} of integrated luminosity, and we investigated the applicability of the helicity discrimination variables. We found that in the case of a 1.5 TeV Z' that can decay into an up quark and a top quark, the top quark helicity can be determined, even for higher momentum cuts. For the Z' model with decays to $\tau^+\tau^-$ we used the τ decay vertex information along with a likelihood method to correct for detector resolution effects, resulting in good discrimination between the left- and right-handed modes for 1 fb^{-1} of integrated luminosity. For the leptoquark pair-production model, for 400 GeV leptoquarks decaying into a top quark and a τ lepton each, we examined reconstruction of the case when both the decaying fully hadronically. Discrimination in this scenario is more challenging, but values of $\chi^2/N_{\text{d.o.f.}} \sim 2 - 3$ can be obtained even with higher than minimal cuts for an integrated luminosity of 100 fb^{-1} .

To summarize, we have assessed the magnitude of the effects of QCD, cuts on the transverse momentum, detector effects and finally the reconstruction issues that arise in this phenomenological study of helicity variables. This work is indicative of the difficulties that arise in ‘measuring’ the helicities to determine the form of the interactions of new particles to quarks and leptons of the third generation. To fully

determine the potential performance of these variables, the next step would be for the experimental collaborations to perform similar analyses once the Large Hadron Collider detector performance is understood.

5. Acknowledgements

We would like to thank the Cavendish Laboratory’s High Energy Physics group for allowing continuous use of their computing facilities, as well as the Cambridge Supersymmetry Working Group for useful suggestions and discussion related to this paper. This research is supported in part by the Swiss National Science Foundation (SNF) under contract 200020-138206 and the Research Executive Agency (REA) of the European Union under the Grant Agreement number PITN-GA-2010-264564 (LHCPhenoNet).

A. Angular variables

A.1 Definitions

We define here two ‘angular’ variables, the first of which is the angle $\theta_{b,\ell}$, defined between the b -quark and the lepton, ℓ , in semi-leptonic top decays as shown in Fig. 27. The angle is defined in the lab frame, but is shown in the figure in the centre-of-mass frame of the decaying top quark for illustration purposes. We consider a function of this variable defined by:

$$f(\cos \theta_{b,\ell}) = 0.25 \times (1 + \cos \theta_{b,\ell}) . \quad (\text{A.1})$$

We will also be considering the distance between the lepton and neutrino for semi-leptonic top decays, given by $\Delta R(\ell, \nu) = \sqrt{\delta\eta_{\ell,\nu}^2 + \delta\phi_{\ell,\nu}^2}$, where $\delta\eta_{\ell,\nu}$ and $\delta\phi_{\ell,\nu}$ are the distances in the pseudo-rapidity, $|\eta_\ell - \eta_\nu|$, and transverse plane angle, $|\phi_\ell - \phi_\nu|$.

A.2 Angular variables in the Z' flavour-changing model

Figures 28 and 29 show the angular variables at parton-level for the Z' model described by the Lagrangian density of Eq. (3.1), for a mass of 1.5 TeV. In Figs. 30 and 31 we show the reconstructed distributions after Delphes simulation for the minimal set of cuts, and Figs. 32 and 33 show the corresponding reconstructed distributions for the set of cuts A and B , defined in section 3.1.2. Table 3 shows the corresponding $\chi^2/N_{\text{d.o.f.}}$ between the left- and right-handed distributions corresponding to the figures. It is evident that these angular variable can provide equivalent magnitudes of discrimination between left- and right-handed top quarks as the energy function variables that have been used throughout the main part of the paper.

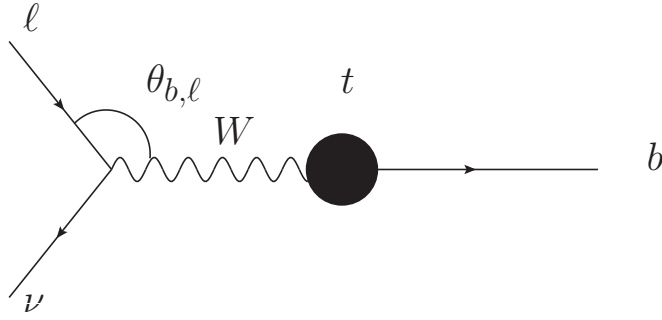


Figure 27: The angle $\theta_{b,\ell}$, between the b quark and lepton in top decay, shown in the centre-of-mass frame of the top for illustration purposes. The angle is calculated in the lab frame throughout this paper.

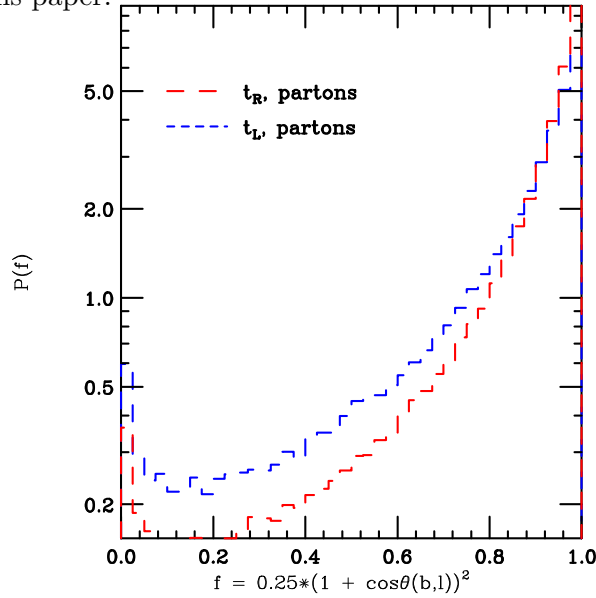


Figure 28: The $f(\cos \theta_{b,\ell})$ variable for left- or right-handed Z' bosons decaying to $u\bar{t}$ or $\bar{u}t$, obtained from parton-level events.

Variable	$\Delta R(\ell, \nu)$	$f(\cos \theta(b, \ell))$
Min.	45.7	29.1
A	35.4	19.1
B	34.0	12.6

Table 3: The value of $\chi^2/N_{\text{d.o.f.}}$ between the left- and right-handed distributions in the Z' scenario for the three different sets of cuts. It is evident that the distributions are distinguishable even for the higher cuts, with the u variable distribution performing well in all cases.

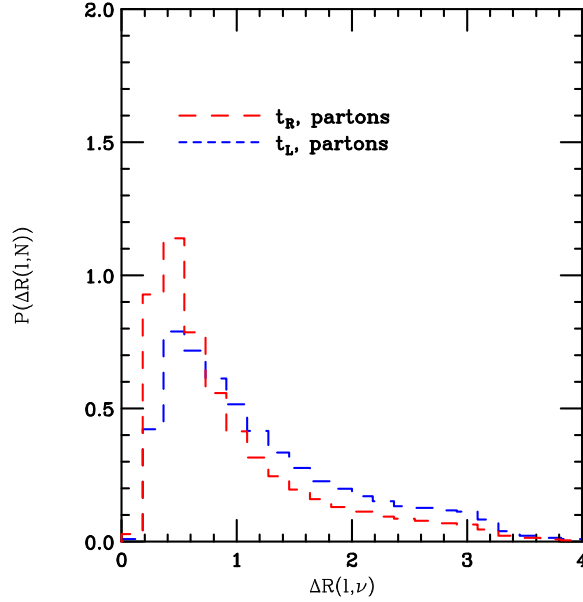


Figure 29: The $\Delta R(\ell, \nu)$ variable for left- or right-handed Z' bosons decaying to $u\bar{\ell}$ or $\bar{u}t$, obtained from parton-level events.

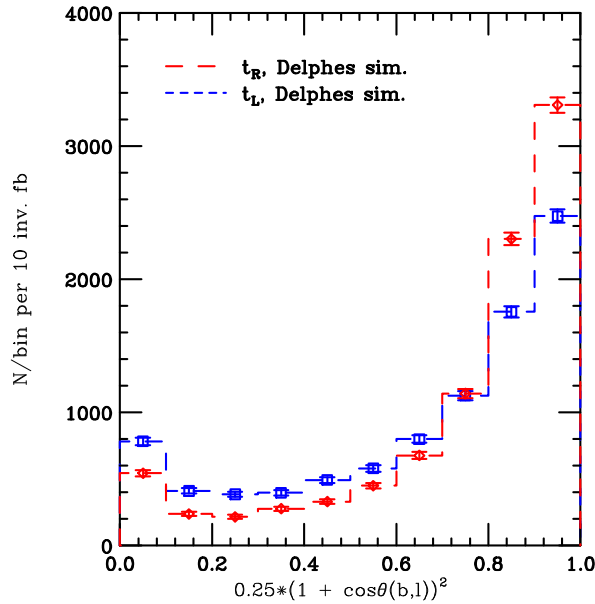


Figure 30: The $f(\cos\theta_{b,\ell})$ variable for a left- or right-handed Z' bosons decaying to $u\bar{\ell}$ or $\bar{u}t$, obtained from the reconstructed events for an LHC run at 14 TeV, with 10 fb^{-1} .

B. The χ^2 between two histograms

For the comparison of two binned data sets, χ^2 can be defined as [15]:

$$\chi^2 = \sum_i \frac{(R_i - S_i)^2}{R_i + S_i}, \quad (\text{B.1})$$

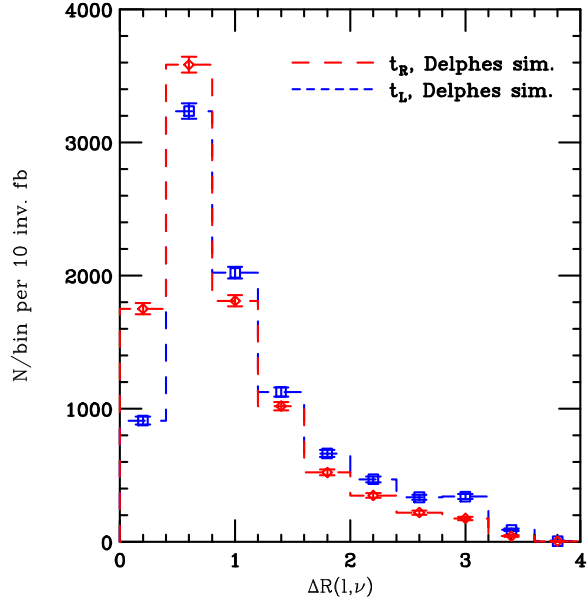


Figure 31: The $\Delta R(\ell, \nu)$ variable for a left- or right-handed Z' bosons decaying to $u\bar{\ell}$ or $\bar{\ell}u$, obtained from the reconstructed events for an LHC run at 14 TeV, with 10 fb^{-1} .

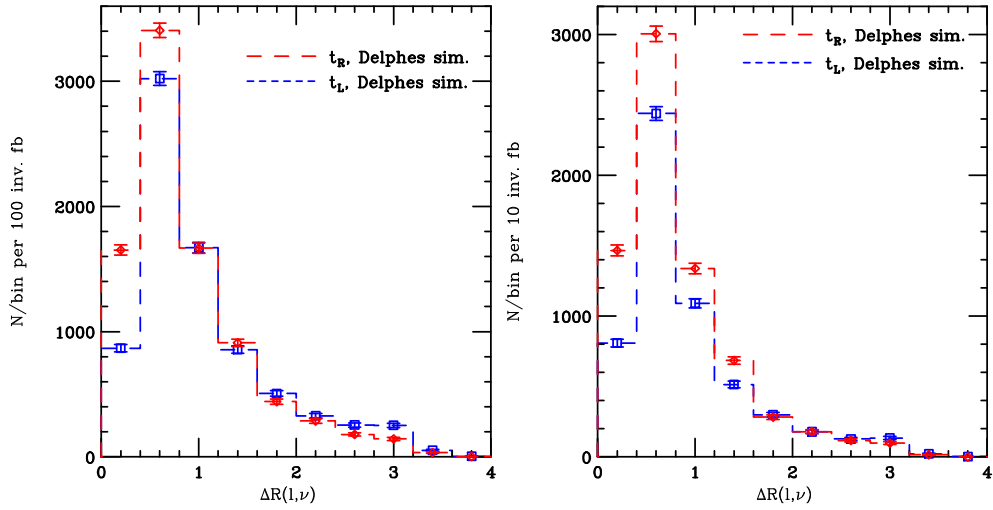


Figure 32: The $\Delta R(\ell, \nu)$ variable for a left- or right-handed Z' bosons decaying to $u\bar{\ell}$ or $\bar{\ell}u$, obtained from the reconstructed events for an LHC run at 14 TeV, with 10 fb^{-1} , with the set of cuts A (left) and B (right), as explained in the text.

where R_i and S_i are the number of events in i^{th} bin of the first and second datasets respectively.

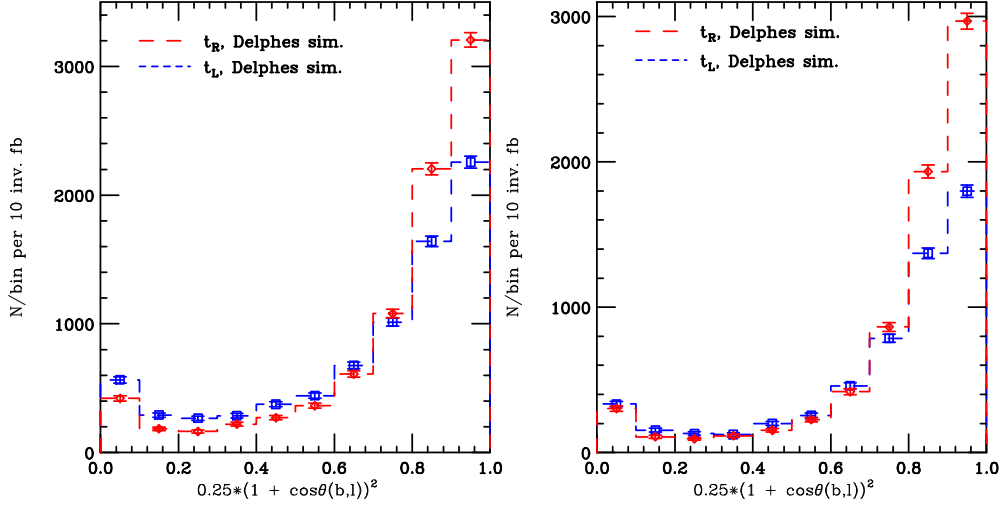


Figure 33: The $f(\cos\theta_{b,\ell})$ variable for a left- or right-handed Z' bosons decaying to $u\bar{t}$ or $\bar{u}t$, obtained from the reconstructed events for an LHC run at 14 TeV, with 10 fb^{-1} , with the set of cuts A (left) and B (right), as explained in the text.

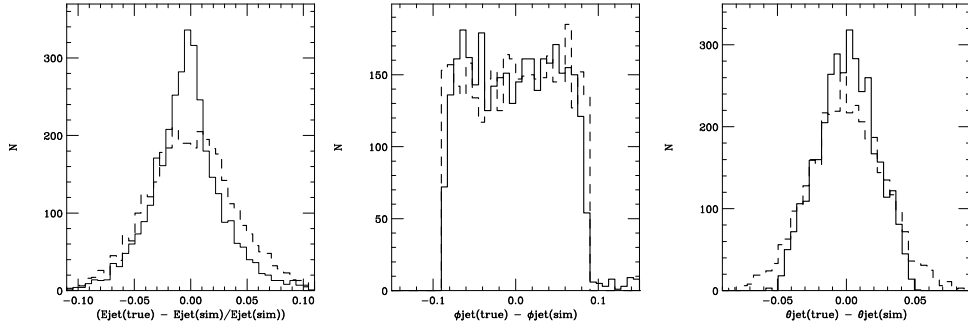


Figure 34: The probability density functions for smearing of jet energy, the angle on the transverse plane ϕ of jets, and the azimuthal angle θ of jets. The solid histograms show the actual Delphes simulation results whereas the dashed one show the functions that were actually used for the likelihood method of section 3.2.

C. Detector-level smearing

The probability density functions used for the likelihood method that corrects for likelihood methods are shown in Fig. 34 and Fig. 35 with dashed histograms. The solid histograms show the actual discrepancy between parton-level and detector-level objects as obtained by Delphes. In practice these distributions would be known features of the detector performance.

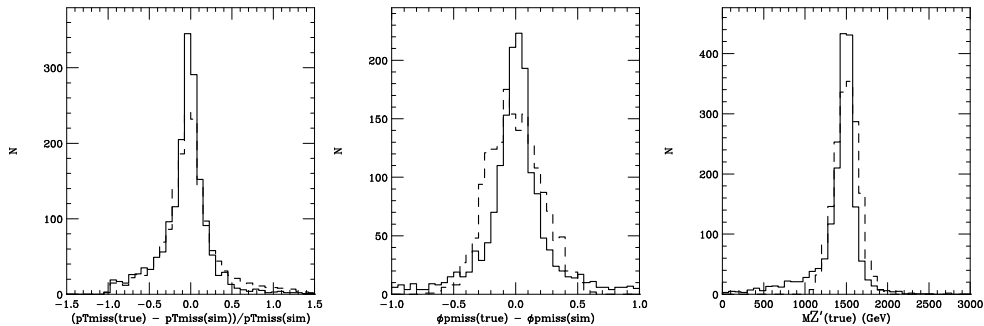


Figure 35: The probability density functions for smearing of missing transverse energy, the angle on the transverse plane, ϕ , of the missing transverse momentum vector, and the actual smearing on the Z' mass distribution (i.e. measured through some other decay mode). The solid histograms show the actual Delphes simulation results whereas the dashed one show the functions that were actually used for the likelihood method of section 3.2.

D. Alternative leptoquark decay: $S_{XY} \rightarrow t_R \bar{\tau}_L, t_L \bar{\tau}_R$

In section 3.3 we considered the decay of a leptoquark which we called S_{XX} , where $X \in \{L, R\}$, with electromagnetic charge $\pm 5/3$ to either $\bar{t}_R \bar{\tau}_R$ or $\bar{t}_L \bar{\tau}_L$. Here we consider the alternative combination of helicities, corresponding to a leptoquark with charge $\pm 1/3$ which we call S_{XY} , where $X \neq Y$ and $X, Y \in \{L, R\}$.¹³ The results for x_{top} and x_τ , for the fully-hadronic leptoquark analysis constructed in section 3.3 are shown in Figs. 36 and Figs. 37 respectively, for the minimal set of cuts. Note that in this case one should understand that the left-handed τ should be paired up with the right-handed top and vice versa (i.e. red in one plot with blue in the other).

The values of $\chi^2/N_{\text{d.o.f.}}$ were found to differ compared to those of the $+5/3$ case, corresponding to ~ 1.6 for the x_τ variable and ~ 8.2 for the x_{top} variable. The differences between the S_{XY} and S_{XX} leptoquarks arise due to the difference in acceptances of the left- and right-handed particles. These are a consequence the interplay of the efficiencies associated with the b -tagging, τ -tagging and reconstruction of the top quarks.

E. Matrix element for polarized top decay

It is useful to outline here the derivation of the polarized top decay differential width. The coupling of the W boson to the fermions is given by:

$$\mathcal{L} = \frac{g}{2\sqrt{2}} V_{ff'} \bar{f} \gamma_\mu (1 - \gamma_5) f' W^\mu + \text{h.c.}, \quad (\text{E.1})$$

¹³In the notation of Ref. [6], we are actually considering the decays of the upper component of the $S_{1/2}$ doublet, $S_{1/2}^{(+)}$.

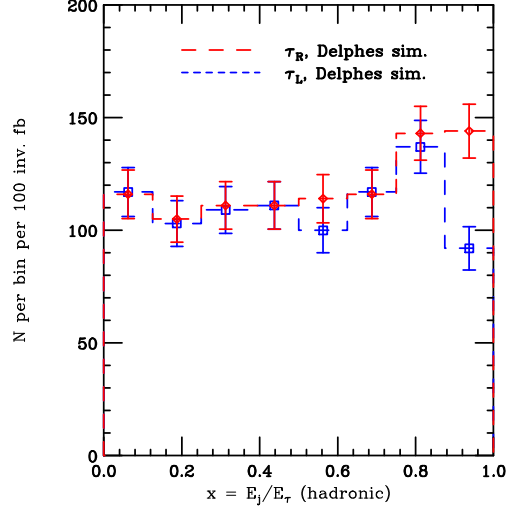


Figure 36: The x_τ variable for left- or right-handed tops from the S_{XY} leptoquark, for an integrated luminosity of 100 fb^{-1} for a 14 TeV LHC.

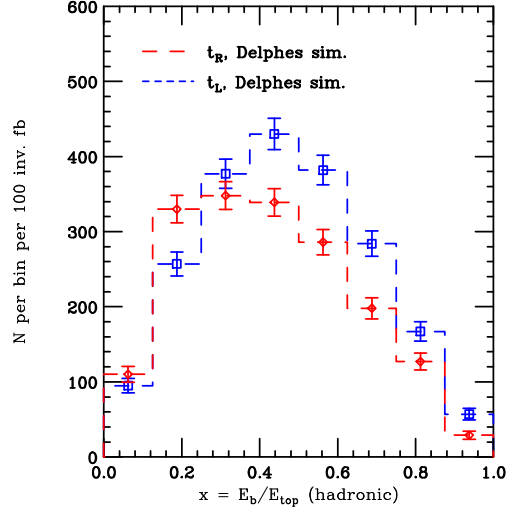


Figure 37: The x_{top} variable for left- or right-handed tops from the S_{XY} leptoquark, for an integrated luminosity of 100 fb^{-1} for a 14 TeV LHC.

where g is the weak charge and $V_{ff'}$ is the CKM matrix element corresponding to the fermions f and f' . The matrix element, corresponding to the diagram shown in Fig. 38 is given by:

$$\mathcal{M} = \frac{g^2}{8} V_{tb} V_{ff'} \bar{u}_b^r(p_2) \gamma_\mu (1 - \gamma_5) W^\mu u_t^s p_1 \bar{u}_{f'}^{r_1}(q_1) \gamma_\nu (1 - \gamma_5) v_f^{r_2}(q_2) W^\nu G(q^2), \quad (\text{E.2})$$

where u and v are the positive and negative frequency spinors, W^μ is the W polarization vector and $G(q^2)$ is the W propagator,

$$G(q^2) = \frac{1}{(q^2 - M_W^2) + i\Gamma_W M_W} . \quad (\text{E.3})$$

Squaring the matrix element and summing over the b quark and fermion spins, we obtain:

$$\begin{aligned} \sum_{r_1, r_2, r} |\mathcal{M}| &= \Omega \text{Tr} \left[\frac{1}{2} (1 + 2s\gamma_5 \not{S}) (\not{p}_1 + m_t) \gamma_k (1 - \gamma_5) \not{p}_2 \gamma_\mu (1 - \gamma_5) \right] \\ &\times \text{Tr} \left[\not{q}_1 \gamma_\nu (1 - \gamma_5) \not{q}_2 \gamma_\lambda (1 - \gamma_5) \right] \\ &\times W^\mu W^\nu W^{*\lambda} W^{*k} , \end{aligned} \quad (\text{E.4})$$

where $S = 1/m_t(|\vec{p}_1|, E_1 \vec{p}_1/|\vec{p}_1|)$ is the spin 4-vector for the top-quark and Ω is defined as:

$$\Omega \equiv \frac{g^4}{64} |V_{tb}|^2 |V_{ff'}|^2 \times \frac{1}{(q^2 - M_W^2)^2 + \Gamma_W^2 M_W^2} . \quad (\text{E.5})$$

The traces can be calculated using the FORM package [16]. The first trace in Eq. (E.4), corresponding to a top quark with spin $s = \pm 1/2$ and the bottom quarks, is given by:

$$\begin{aligned} &4 (p_1^\mu p_2^k + p_1^k p_2^\mu - g^{\mu k} p_1 \cdot p_2 - \epsilon^{ij\mu k} p_1^i p_2^j) \\ &+ 8 m_t s (-p_2^\mu S^k - S^\mu p_2^k + g^{\mu k} p_2 \cdot S - \epsilon^{ij\mu k} p_2^i S^j) . \end{aligned} \quad (\text{E.6})$$

Is obvious that the second term in the above result vanishes if we sum over s or set $m_t \rightarrow 0$. The second trace in Eq. (E.4), corresponding to the fermions f and f' is given by:

$$8(q_1^\nu q_2^\lambda + q_1^\lambda q_2^\nu - g^{\nu\lambda} q_1 \cdot q_2 + 8\epsilon^{ij\mu k} q_1^i q_2^j) . \quad (\text{E.7})$$

Summing over the W polarizations introduces $g^{k\lambda}$ and $g^{\mu\nu}$, and gives, for the polarized top matrix element squared,

$$|\mathcal{M}|^2(s) = 128\Omega(p_2 \cdot q_1) [(p_1 - m_t(2s)S) \cdot q_2] . \quad (\text{E.8})$$

F. Finite mass effects on top polarization

F.1 Production polarization

We adapt the description given in Ref. [4] for the case of stop decay to a top and a neutralino, to the decay of a scalar leptoquark to a top and another fermion. The

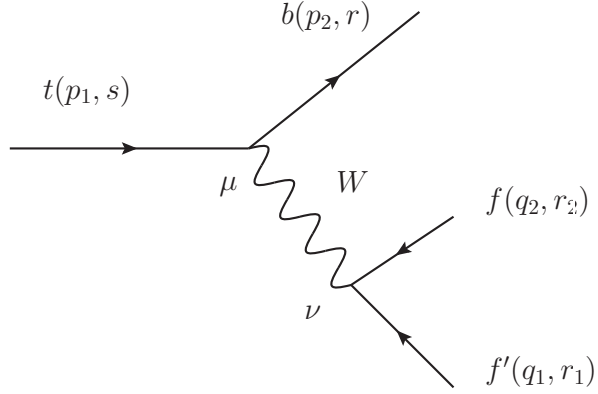


Figure 38: The Feynman diagram for polarized top decay. The parentheses indicate the 4-momentum and spin labels respectively, for each particle.

corresponding Lagrangian for the decay of scalar leptoquark S to $t_{L,R}$ and a fermion f can be written as:

$$\mathcal{L} = g_L t_L S f + g_R t_R S f + \text{h.c.} , \quad (\text{F.1})$$

where g_L and g_R are the left- and right-handed couplings respectively. The axis of spin quantization is taken to lie along the top direction of motion in the parent leptoquark rest frame. The production amplitudes for positive and negative helicity top quarks depend on two functions F_{\pm} :

$$F_{\pm} = \frac{(E_t + m_t \pm |p_t|)(E_f + m_f \pm |p_f|)}{4(E_t + m_t)(E_f + m_f)} , \quad (\text{F.2})$$

where all quantities are given in the leptoquark rest frame. The functions result from explicit evaluation of the matrix element for the leptoquark decay using the spinor wavefunctions. These are given by:

$$u(\vec{p}, s) = \begin{pmatrix} \sqrt{p \cdot \sigma} \chi_s \\ \sqrt{p \cdot \bar{\sigma}} \chi_s \end{pmatrix} , \quad v(\vec{p}, s) = \begin{pmatrix} 2s \sqrt{p \cdot \sigma} \chi_{-s} \\ -2s \sqrt{p \cdot \bar{\sigma}} \chi_{-s} \end{pmatrix} , \quad (\text{F.3})$$

where the spinors χ_s are eigenstates of the operator $1/2 \vec{\sigma} \cdot \hat{s}$ with eigenvalue s and are given, for \hat{s} along the z -direction, by:

$$\chi_{1/2}(\hat{z}) = \begin{pmatrix} 1 \\ 0 \end{pmatrix} , \quad \chi_{-1/2}(\hat{z}) = \begin{pmatrix} 0 \\ 1 \end{pmatrix} . \quad (\text{F.4})$$

For the decay of a scalar to left-handed tops, for example, the matrix element is proportional to $\bar{v}(\vec{p}, s) P_L u(\vec{k}, r)$, where \vec{p} and s are the top momentum and spin respectively, and \vec{k} and r are the fermion momentum and spin respectively. The P_L operator projects the upper component of $u(\vec{k}, r)$ and hence the matrix element for the left-handed coupling is given by:

$$\mathcal{M}_s^L \propto \begin{pmatrix} -2s \sqrt{p \cdot \bar{\sigma}^\dagger} \chi_{-s} & 2s \sqrt{p \cdot \bar{\sigma}^\dagger} \chi_{-s} \end{pmatrix} \begin{pmatrix} -2s \sqrt{p \cdot \bar{\sigma}^\dagger} \chi_{-s} \\ 0 \end{pmatrix} . \quad (\text{F.5})$$

Using the relations [?]:

$$\begin{aligned}\sqrt{p \cdot \sigma} &= \frac{(E_p + m)\mathbb{I} - \vec{\sigma} \cdot \vec{p}}{\sqrt{2(E_p + m)}}, \\ \sqrt{p \cdot \bar{\sigma}} &= \frac{(E_p + m)\mathbb{I} + \vec{\sigma} \cdot \vec{p}}{\sqrt{2(E_p + m)}},\end{aligned}\tag{F.6}$$

we obtain the following:

$$\mathcal{M}_s^L \propto -2s\chi_{-s}^\dagger \frac{[(E_t + m_t)\mathbb{I} + \sigma \cdot \vec{p}][\vec{\sigma} \cdot \vec{k}]}{\sqrt{4(E_t + m_t)(E_f + m_f)}}\chi_r.\tag{F.7}$$

Since we are interested only in the top polarization, s , we can sum over the fermion polarization, r , replacing χ_r with a column vector with unit entries, $(1, 1)$. If we define, $D \equiv \sqrt{4(E_t + m_t)(E_f + m_f)}$, then

$$\mathcal{M}_s^L \propto -\frac{2s}{D}\chi_{-s}^\dagger \begin{pmatrix} E_t + m_t + p_z & p_x - ip_y \\ p_x + ip_y & E_t + m_t - p_z \end{pmatrix} \begin{pmatrix} E_f + m_f - k_z & -k_x + ik_y \\ k_x + ik_y & E_f + m_f + k_z \end{pmatrix} \begin{pmatrix} 1 \\ 1 \end{pmatrix}.\tag{F.8}$$

In the rest frame of the scalar leptoquark, we take the z -axis to lie along the top direction of motion, and hence we have $p_x = p_y = k_x = k_y = 0$ and $p_z = -k_z$ and the matrix element finally becomes:

$$\mathcal{M}_s^L \propto -\frac{2s}{D}\chi_{-s}^\dagger \begin{pmatrix} E_t + m_t + p_z & 0 \\ 0 & E_t + m_t - p_z \end{pmatrix} \begin{pmatrix} E_f + m_f - k_z \\ E_f + m_f + k_z \end{pmatrix}.\tag{F.9}$$

Thus, setting $s = +1/2$ picks the upper element of the resulting column matrix, whereas $s = -1/2$ picks the lower element of the matrix. It is easy to see that the functions F_\pm arise naturally then. The extension to \mathcal{M}_s^R is trivial, and the resulting matrix elements are thus given by:

$$\mathcal{M}_\pm^L \propto g_L F_\mp, \quad \mathcal{M}_\pm^R \propto g_R F_\pm.\tag{F.10}$$

For finite m_t this gives a non-vanishing amplitude for top quarks of both helicities even in the limit of a purely chiral vertex. The polarization along the production axis is given by:

$$\langle P_P \rangle = \frac{(|g_R|^2 - |g_L|^2)M_{LQ}|p_t|}{(|g_R|^2 + |g_L|^2)(M_{LQ}E_t - m_t^2) + 2g_R g_L m_f m_t},\tag{F.11}$$

where M_{LQ} is the leptoquark mass. The effect is small if the top is produced in association with a light fermion, e.g. in the case of leptoquark decay to $t\tau$.¹⁴

¹⁴Note that it may be interesting to investigate whether the helicity distributions of the top can provide independent information on the mass of the accompanying sister particle, especially if this is weakly-interacting (and hence invisible).

F.2 Polarization axis rotation effects

The natural polarization axis for reconstructed tops is their direction of motion. This is referred to as the detection axis in Ref. [4]. The most natural observable for hadronic tops is then the angular distribution of the b quark jets with respect to the top quark direction of motion in the the top rest frame,

$$\frac{1}{\Gamma} \frac{d\Gamma}{d \cos \theta'} = \frac{1}{2} (1 + \langle P_D \rangle \kappa \cos \theta'), \quad (\text{F.12})$$

where $\langle P_D \rangle$ is the observed polarization along the detection axis. In general, the detection axis and the production axis are at an angle ω :

$$\langle P_D \rangle = \langle P_P \rangle \cos \omega. \quad (\text{F.13})$$

This angle is the Wigner angle determined by the composition of boosts from the top rest frame to the lab frame, followed by a boost from the lab frame to the top's parent rest frame and finally a boost from the parent rest frame to the top rest frame. From this composition of boosts it is found that [4]:

$$\cos \omega = \frac{E_t \beta_p \cos \theta + |p_t|}{\sqrt{|p_t|^2 (1 + \beta_p^2 \cos^2 \theta) + m_t^2 \beta_p^2 + 2 E_t |p_t| \cos \theta}} \quad (\text{F.14})$$

where E_t , p_t are the energy and momentum of the top in the parent rest frame, θ is the angle of the top in the parent rest frame, and β_p is the boost between the parent rest frame and the lab frame. For a given model distributions of boosts $P(\beta_p)$ can be calculated from the dynamics and the PDFs and the detection polarization can be derived by:

$$\langle P_D \rangle = \langle P_P \rangle \frac{1}{2} \int d \cos \theta d \beta_p P(\beta_p) \cos \omega(\theta, \beta_p). \quad (\text{F.15})$$

For sufficiently heavy parent particles, $\beta_p \sim 0$ and $\cos \omega \sim 1$, as there will be little difference between the production and detection axes.

If both the boost of the daughter top quark $\beta_t \neq 1$ and the boost of the parent $\beta_p \neq 0$, then the full two-dimensional distribution of the two boosts has to be used. The detected polarization can then be calculated on an event-by-event basis by first choosing β_p from the integrated distribution over β_t and then using:

$$\langle P_D \rangle = \langle P_P \rangle \frac{1}{2} \int d \cos \theta \cos \omega(\theta, \beta_p). \quad (\text{F.16})$$

The subsequent boost of the top quark can then be sampled from $P(\beta_p, \beta_t)$, using the fixed β_p . Note that in the case of the flavour-changing Z' considered in this paper, $\cos \omega = 1$ since the production and detection frames of the top are identical. This can be understood clearly if one considers in this case the composition of boosts described below Eq. (F.14): the boosts would all be parallel, returning to the same point without rotation.

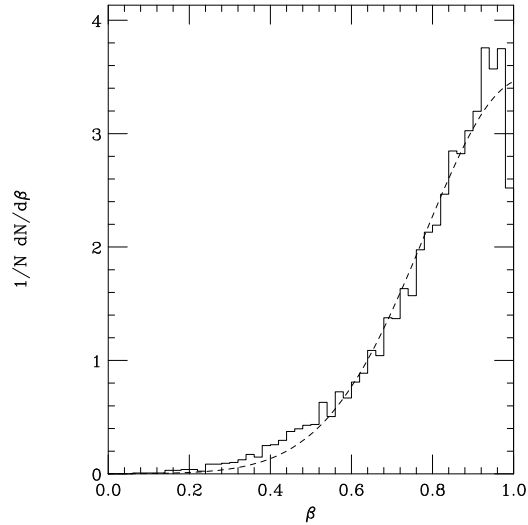


Figure 39: The fit to the top quark β_t distribution for 400 GeV leptoquarks is shown in solid black dashes. The HERWIG++ histogram extracted from parton-level Monte Carlo events is shown in solid black.

F.3 β distributions from Monte Carlo

We also show the form of the two-dimensional $\beta_p - \beta_t$ distribution for 400 GeV leptoquarks, extracted from the HERWIG++ event generator in Fig. 40. For the β_t

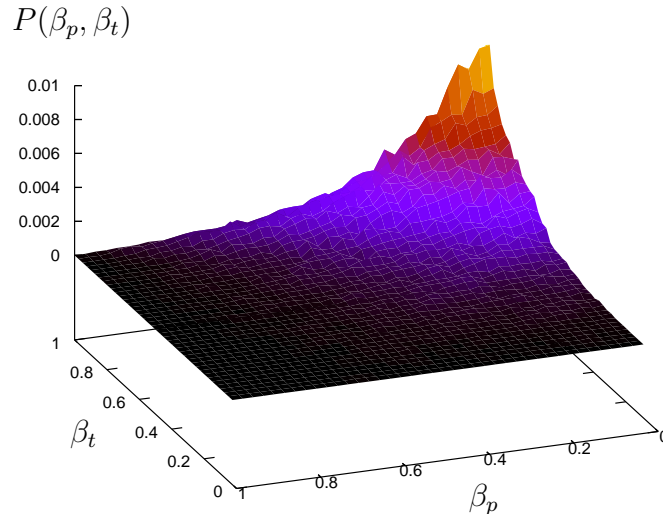


Figure 40: The $\beta_p - \beta_t$ distribution for 400 GeV leptoquarks, extracted from the HERWIG++ event generator, is shown.

distribution (i.e. integrated over β_p) in the decay of a 400 GeV leptoquark a fit can

be made, shown in Fig. 39. The fit has the form of a Gaussian:

$$P(\beta_t) = a \exp(-(\beta_t - b)^2/c) \quad , \quad (\text{F.17})$$

where the parameters a , b and c were given by the fit to be $a \simeq 3.48$, $b \simeq 1.03$, $c \simeq 0.13$. The distribution integrates to ~ 1 in $\beta_t \in (0, 1)$.

References

- [1] B. Gripaios, “Composite Leptoquarks at the LHC,” *JHEP* **1002** (2010) 045, 0910.1789.
- [2] M. Jezabek and J. H. Kuhn, “Lepton Spectra from Heavy Quark Decay,” *Nucl.Phys.* **B320** (1989) 20.
- [3] A. Czarnecki, M. Jezabek, and J. H. Kuhn, “LEPTON SPECTRA FROM DECAYS OF POLARIZED TOP QUARKS,” *Nucl.Phys.* **B351** (1991) 70–80.
- [4] J. Shelton, “Polarized tops from new physics: signals and observables,” *Phys.Rev.* **D79** (2009) 014032, 0811.0569.
- [5] S. Gieseke, D. Grellscheid, K. Hamilton, A. Papaefstathiou, S. Platzer, *et al.*, “Herwig++ 2.5 Release Note,” 1102.1672.
- [6] B. Gripaios, A. Papaefstathiou, K. Sakurai, and B. Webber, “Searching for third-generation composite leptoquarks at the LHC,” *JHEP* **1101** (2011) 156, 1010.3962.
- [7] R. M. Godbole, L. Hartgring, and I. N. C. D. White, “Top polarisation studies in H^-t and Wt production,” 1111.0759. * Temporary entry *.
- [8] S. Oryn, X. Rouby, and V. Lemaître, “DELPHEES, a framework for fast simulation of a generic collider experiment,” 0903.2225.
- [9] P. Bellan, “Measurements of Inclusive b-quark Production at 7 TeV with the CMS Experiment,” 1109.2003.
- [10] G. P. Salam, “Towards Jetography,” *Eur.Phys.J.* **C67** (2010) 637–686, 0906.1833.
- [11] J. D. Anderson, M. H. Austern, and R. N. Cahn, “Measurement of Z-prime couplings at future hadron colliders through decays to tau leptons,” *Phys.Rev.* **D46** (1992) 290–302.
- [12] A. Elagin, P. Murat, A. Pranko, and A. Safonov, “A New Mass Reconstruction Technique for Resonances Decaying to di-tau,” *Nucl.Instrum.Meth.* **A654** (2011) 481–489, 1012.4686. * Temporary entry *.
- [13] B. Gripaios, K. Sakurai, and B. Webber, “Polynomials, Riemann surfaces, and reconstructing missing-energy events,” *JHEP* **1109** (2011) 140, 1103.3438.

- [14] T. Plehn, M. Spannowsky, and M. Takeuchi, “How to Improve Top Tagging,” 1111.5034. * Temporary entry *.
- [15] W. H. Press, S. A. Teukolsky, W. T. Vetterling, and B. P. Flannery, *Numerical Recipes: The Art of Scientific Computing*. Cambridge University Press, UK, third edition ed., 2007.
- [16] J. Vermaseren, “New features of FORM,” math-ph/0010025.